Distribution of T-type calcium channels in LGN interneurons

Joy-Loi Chepkoech

Norwegian University of Life Sciences
Department of Mathematical Sciences and Technology
Master Thesis 60 credits 2012

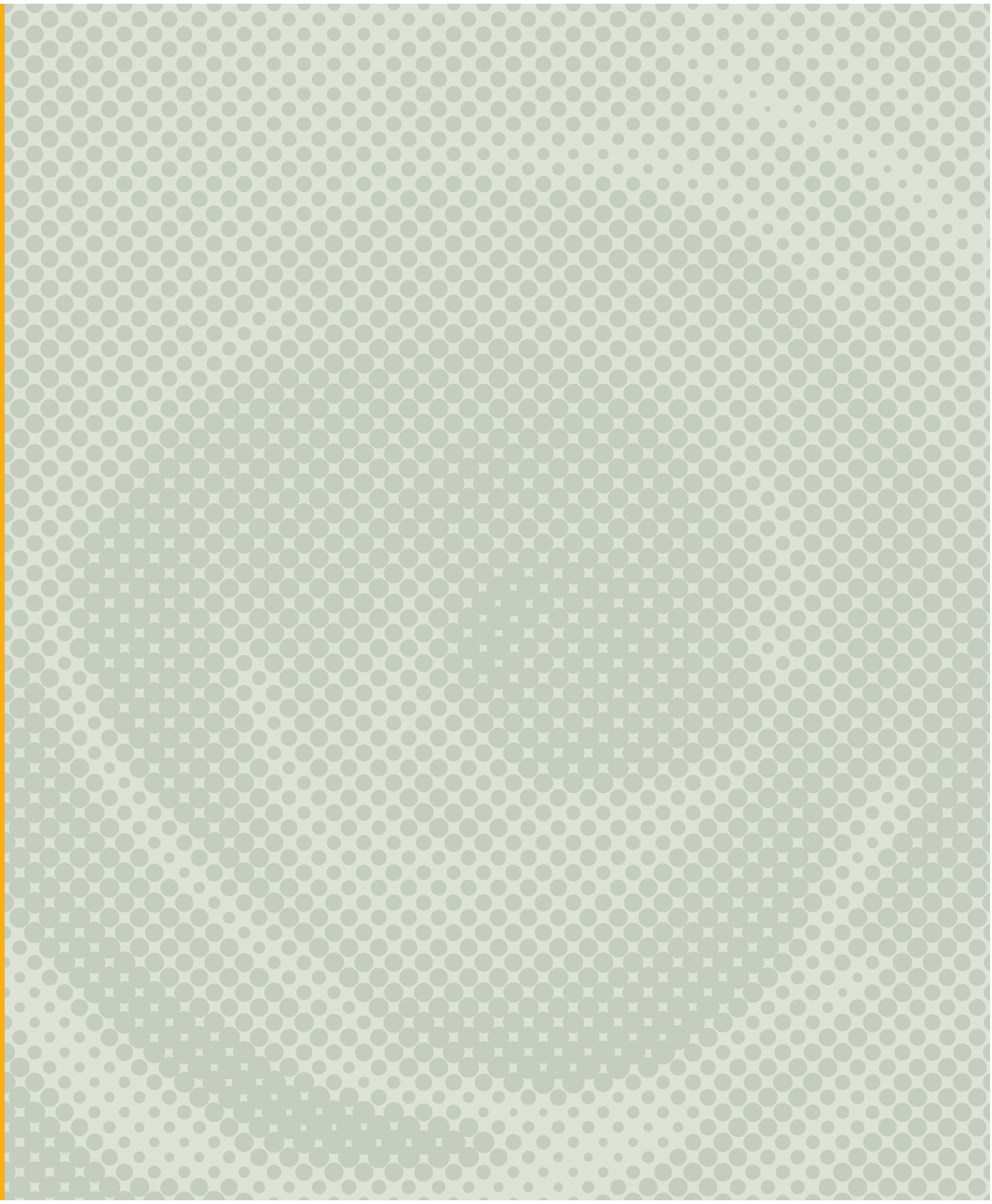

Preface

This thesis would not have been completed without the solid guidance of Geir Halnes. Through every part of the process, he has provided immense knowledge and support, and readily answered all my questions.

Wonderful friends have helped cheer me on in a period that has been tough (thank you Sigrid, Sigrid, Ana, Ine and Ståle!), and I will miss the hours spent at my office spot in the warm home of Tore and Ann-Jorunn.

I could not wish for a more unconditionally patient and present family than Gard and mummy. Mummy, we did it!

Oslo, May 11, 2012

Abstract

The retina of the eye receives visual information that is passed on by the lateral geniculate nucleus (LGN). LGN is the relay centre of the brain, and has two types of neurons: interneurons (INs) and thalamocortical neurons (TCNs). INs form inhibitory synapses on the TCNs, and have presynaptic terminals in the dendrites as well as the soma. These various locations of sites make them special, and somatic IN activity may thus be a result of either axonal or dendritic GABA release onto TCNs.

Dendritic sites of GABA release are most often located in the distal dendrites of the INs, as part of triadic synapses elsewhere in the brain. In these triads, both presynaptic and postsynaptic terminals of INs lie close to each other. If a terminal receives strong enough visual input from retinal ganglion neurons (RGNs), GABA release can be locally triggered at the very same site without somatic involvement. GABA release from these dendritic sites may also be triggered by somatic activity of INs.

The function of having multiple release possibilities is not fully understood, and neither are the conditions for GABA release in these sites. In order to gain understanding of this, more knowledge of the two-way communication between distal dendrites and the soma is crucial.

T-type calcium channels (I_T-channels) are important for achieving firing in thalamic cells. The distribution of I_T-channels on the somatodendritic membrane has been suggested to be important for the cell functions [10]. In a modeling study of TCNs, it was concluded that specific I_T-channel distributions were optimal for the TCNs ability to evoke bursts [18]. To my knowledge, no corresponding studies of I_T-channel distributions in INs have been done. Compared to TCNs, INs have relatively long dendrites, and due to their roles as both sender and receiver of signals, the distribution of I_T-channels will likely be important for the INs somatic firing properties, and perhaps more so for the two-way signaling between the soma and the distal dednrites.

In this thesis, I explore what role the I_T-channel distribution plays on the function of INs, using a multicompartmental model of a IN in the LGN. My model is a simplified version of one that was previously developed of a LGN IN, that included 7 ion channels and was able to reproduce qualitative features of various firing properties of INs [9]. The simplified version includes only 3 of these ion channels, as they are most relevant for the questions I wish to pose.

Four different distributions of I_T-channels were tested: a linearly increasing distribution g_{lin}, a uniform distribution g_{uni}, a distribution with all the I_T-channels located in the soma g_{zero}, and a stepwise distribution g_{Zom}. Simulations were run for each case, with the intention of exploring the propagation of a somatic signal to the distal dendrites, and how synaptic input at distal dendritic sites gave rise to voltage and calcium elevations in the soma.

I investigated how the I_T-channel distribution affected:

- Somatic voltage and calcium concentration levels in response to somatic input
- Synaptic strengths needed to evoke somatic action potential
- Somatic voltage and calcium concentration levels in response to synaptic input to the distal dendrites
- Distal dendritic voltage and calcium concentration levels in response to somatic input

Finally, a conclusion could be reached that the I_T-channel distribution is more important for the propagation of a signal across the dendrites than it is for somatic firing properties: redistribution of I_T-channels only gave rise to slight changes of the somatic firing signal response to somatic input. However, for dendritic signaling, the responses to both somatic and synaptic signal input varied largely for different distributions of I_T-channels.

Contents

Preface i
Abstract ii

1 Introduction **1**

2 Physiological background **3**
2.1 The nervous system 3
2.1.1 Thalamus 3
2.1.2 LGN 4
2.2 Neurons 5
2.2.1 General neural functions 5
2.2.2 Interneurons in LGN 6
2.2.3 T-type calcium channels in INs 8

3 Computational Background **11**
3.1 Cable modeling 11
3.2 Ion channels 13
3.2.1 Hodgkin Huxley formalism 14
3.2.2 GHK formalism 16
3.2.3 Intracellular calcium concentration 17
3.3 Compartmental neural models 18
3.3.1 Principles of compartmental neuron models 18
3.3.2 A mathematical representation 19
3.4 NEURON simulator 20
3.4.1 Creating the compartmental model using the NEURON simulator 20

4 Methods **23**
4.1 The reduced Halnes et al. model 23
4.1.1 Morphology 23
4.1.2 Passive properties 24
4.1.3 Ion channel kinetics 25
4.1.4 Calcium pool 26
4.2 Model parameters that were varied 26
4.2.1 T-cannel distributions 26
4.2.2 Normalization of gT 28
4.3 Modeling a synapse 28
4.4 Inputs to the model 29

5 Results 31
5.1 Model calibration . . . 31
5.2 How the somatic response to somatic current injection depends on I_T-distributions . . . 33
5.3 Signal propagation in the dendrite depends on I_T-distribution . . . 34
5.3.1 AP propagation did not depend strongly on I_T-channel distribution 37
5.3.2 I_T-distribution greatly affects propagation of calcium spikes and EPSPs . . . 38
5.3.3 Somatic and dendritic responses of synapses in distal dendrites 38

6 Discussion 41
6.1 Main conclusions . . . 41
6.2 Reducing the morophology . . . 41
6.3 Limitations of the study . . . 42
6.4 Comparing results to experimental findings . . . 42
6.5 Future work . . . 43

A HOC code for NEURON Simulations 47
A.1 it2.mod . . . 47
A.2 loi04.hoc . . . 50

Chapter 1

Introduction

Many problems remain unsolved in the vast field of neuroscience. In computational neuroscience, the nervous system is modeled at different structural scales in attempt to better understand the information properties of neural signals [8]. Studies range from large scale, typically addressing statistical properties of networks that consist of thousands or millions of neurons, down to simulations on the scale of single ion channels in a single neuron.

In this thesis, the focus is of rather small scale, aiming to investigate a specific problem that is relevant for a specific cell type in a specific region of the brain.
Visual information is received by the retina of the eye, and is passed on by the brain's relay centre, the lateral geniculate nucleus (LGN). We want to explore interneurons, one of two cell types in the LGN, and hope to gain a better understanding of how the signaling between the soma and the distal dendrites of an interneuron depends on the distribution of calcium ion channels.

The brain consists of many neuron types with properties that vary in similarity, and several of these neurons have T-type calcium channels. This study focuses on the importance of the distribution of T-type calcium channels in interneurons in the LGN. Although the focus is specific, the results may shed light on the general function of the distribution of T-type calcium channels.

Chapter two and three present the physiological and computational background for this thesis. Based on previous literature, they build a basis for understanding this study. In chapter four, the construction of the model, and the simulation setup is described, while chapter five presents the results of simulation. Finally, chapter six offers a discussion of the results.

Chapter 2

Physiological background

2.1 The nervous system

The brain consists of many regions, all with different functions. Neural structures contained in the somatic nervous system are responsible for the conveyance and processing of information (touch, visual, etc...) to the central nervous system which comprises the brain and the spinal cord [4]. Important for this process is a large, egg-shaped mass known as the thalamus, of which a brief introduction follows, with emphasis on the thalamic nuclei LGN which is the focus of this study.

2.1.1 Thalamus

The thalamus is the gateway to the cerebral cortex, a relay centre through which most messages that form a basis for what we know about the outside world and ourselves pass [20].

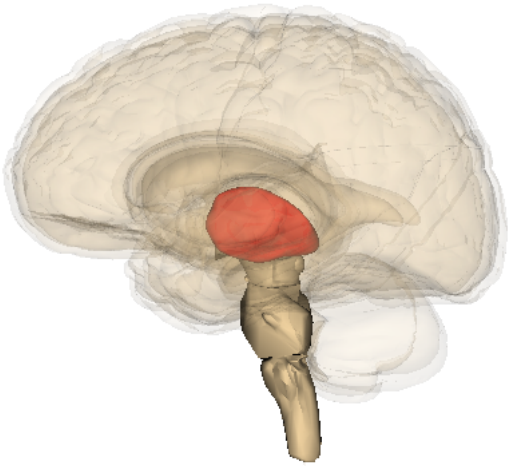

Figure 2.1: The thalamus (marked orange) is located near the centre of the brain. Image from [7]

A small structure on each side of the brain's midline, is assembled of several distinct cell groups that transmit a distinctive type of signal to designated areas in the cerebral cortex (mostly to the neocortex) [20].
The dominant afferents of some of the thalamic nuclei have been identified; ascending pathways concerned with auditory stimuli go to the medial geniculate nucleus, somatosensory stimuli to the ventral posterior nucleus and visual stimuli to the lateral geniculate nucleus. Thalamocortical neurons (TCNs) pass messages to the cortex, and are therefore viewed as *drivers* (as opposed to *modulators*, which is what one calls afferents that can modify (but are not responsible for) the qualitative nature of the messages that are conveyed to the cortex) [20].

2.1.2 LGN

Most of the sensory information received by the brain is communicated through the thalamus of mammals, and to the cerebral cortex. In turn, the cerebral cortex forms feedback connections to the thalamus.

The lateral geniculate nucleus (LGN) in the thalamus receives visual input from retinal ganglion cells (RGNs), processes this information and sends it to the visual cortex. In this processing, receptive fields are refined and visual input is temporally decorrelated. The LGN has traditionally been viewed as the principle mediator between the

retina and the cortex [20].

Only two types of neurons exist in the LGN. About 75% of the neurons are excitatory thalamocortical neurons (TCNs), and the remaining 25% are inhibitory interneurons. Input from retinal ganglion cells (RGNs) is received by TCNs, then processed and passed on to the cortex. This relay process is affected by several factors, including input from INs located in the LGN, a modulatory process in which INs inhibit TCNs [20]. These INs will be the main focus of this study.

2.2 Neurons

2.2.1 General neural functions

Unless otherwise specified, the following sections on neurons are based on the book "The Human Nervous System - Structure and Function" by Charles R. Noback et al. [4].

Neurons - the basic units of nervous systems - consist of a *soma* (cell body) which contains the nucleus (with DNA and other nuclear organelles), and projects an *axon*, a single nerve process that ends at *presynaptic terminals*. The soma also has branching processes called *dendrites*. Dendrites receive neural signals for interneural communication while axons are channels for conducting messages (*action potentials*) to presynaptic terminals at which the neuron is in synaptic contact with other neurons, making it a part of the network that is the nervous system. The construction of a neuron enables it to react to stimuli with an excitation that it rapidly transmits to other parts.

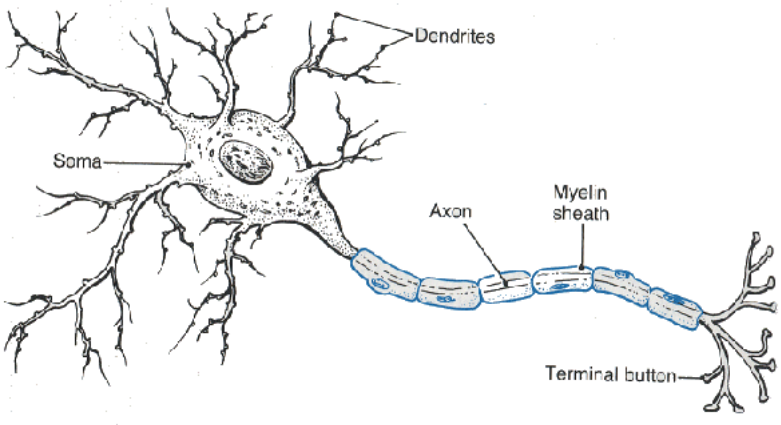

Figure 2.2: Diagram of a neuron, showing its principle parts: axons, . Image from [6]

Communication

A neuron at rest is a charged cell that does not conduct a nerve impulse. Electric charge across the plasma membrane (boundary between extracellular and intracellular fluid) is a result from a thin film of ions (Na^+, Cl^-, K^+) that diffuse across the membrane

along concentration gradients. Synaptic input is received and integrated by neurons. The axons of a neuron carry information from the dendritic cell to synapses, junctions across which impulses pass, enabling communication with other neurons.

Action potentials

Neurons communicate through electrical signals. These signals are generated through the systematic (often voltage dependent) opening and closing of specific ion channels. The stereotypical signaling unit is the action potential (AP). The AP is a fluctuation in the membrane potential. An action potential lasts about 1 ms, and is a roughly 100 mV fluctuation caused by the neuron being depolarized enough to raise the membrane potential above a threshold level, thus initiating a positive feedback process. [8]. It is generated by the rapid opening and closing of Na^+ and K^+ channels. Typically, the neuron will initiate generation of APs when the voltage crosses a certain threshold (this will often be due to synaptic input).

In addition to the typical AP-generating Na^+ and K^+ channels, other channels exist which determine other aspects of neural signaling. The most important one for this study is the T-type Ca^{2+} channel. Here, a slower depolarization may be generated by a transient Ca^{2+} conductance. This depolarization is called a calcium spike, and causes the firing of a burst of action potentials in the neuron. These action potentials are sodium spikes that ride on a slower calcium spike [8].

2.2.2 Interneurons in LGN

Nerve cells of the thalamus are distinguished by their position, connection and morphology. Often, the cells' position in the thalamic nucleus is related to their connections (inputs and outputs, knowledge of which is key to understanding the functional pathway that the cell is a part of), while their morphology is related to their specific functional role (electrical properties and distribution of afferents on cell surface) within the relay pathway [20].

One classification of cells in the dorsal thalamus distinguishes between TCNs that have projection axons, from INs that have locally branching axons.

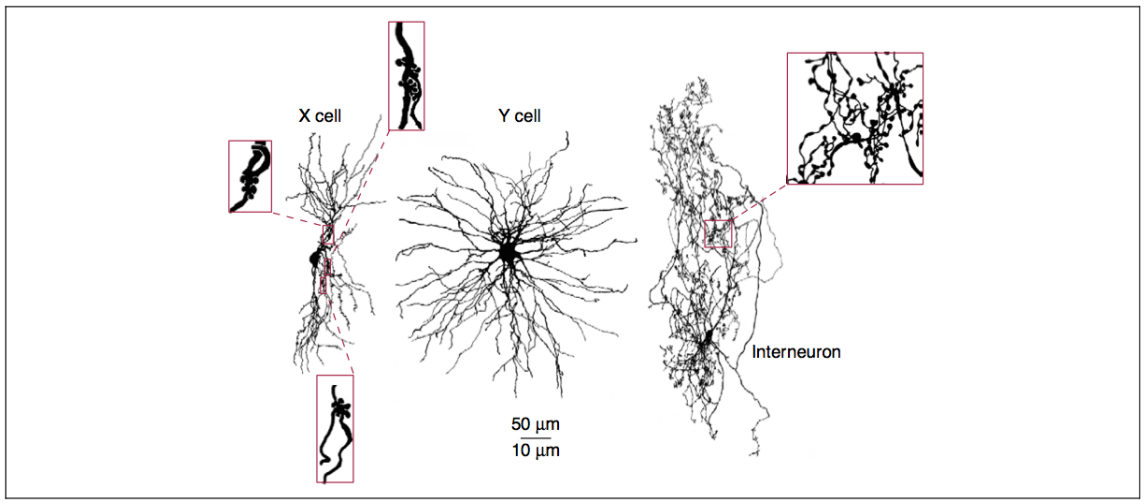

Figure 2.3: Representative cells of the cat LGN. Shown are relay X and Y cells (TCNs) and an interneuron. Insets for the X cell show appendages near proximal branch points, and for the IN shows the numerous swellings that are the presynaptic terminals. Image from [19]

The signaling process of TCNs is affected by inhibition from INs [19]. This inhibition occurs when presynaptic terminals release the neurotransmitter GABA into the synaptic cleft, which then binds to the postsynaptic site of the receiving neuron (which in this case is the TCN). GABA tends to lead to a lowering of membrane potential, making the neuron less likely to fire action potentials.

Two aspects of the IN make it special: firstly, the dendrites have both post- and presynaptic terminals, whereas most neurons only receive input through their dendrites, and transmit it through their axon. Thus, IN inhibition of TCNs can occur through both dendritic and axonal outputs [19].
Secondly, the dendritic synapses that INs form on TCNs often occur in triads at the distal sites of the INs where, both presynaptic and postsynaptic terminals of INs lie close to each other. When a terminal receives a visual input signal that is strong enough form RGNs, GABA release is locally triggered. This triggering occurs at the same sight of the input. Release may also be triggered by somatic IN activity [19].

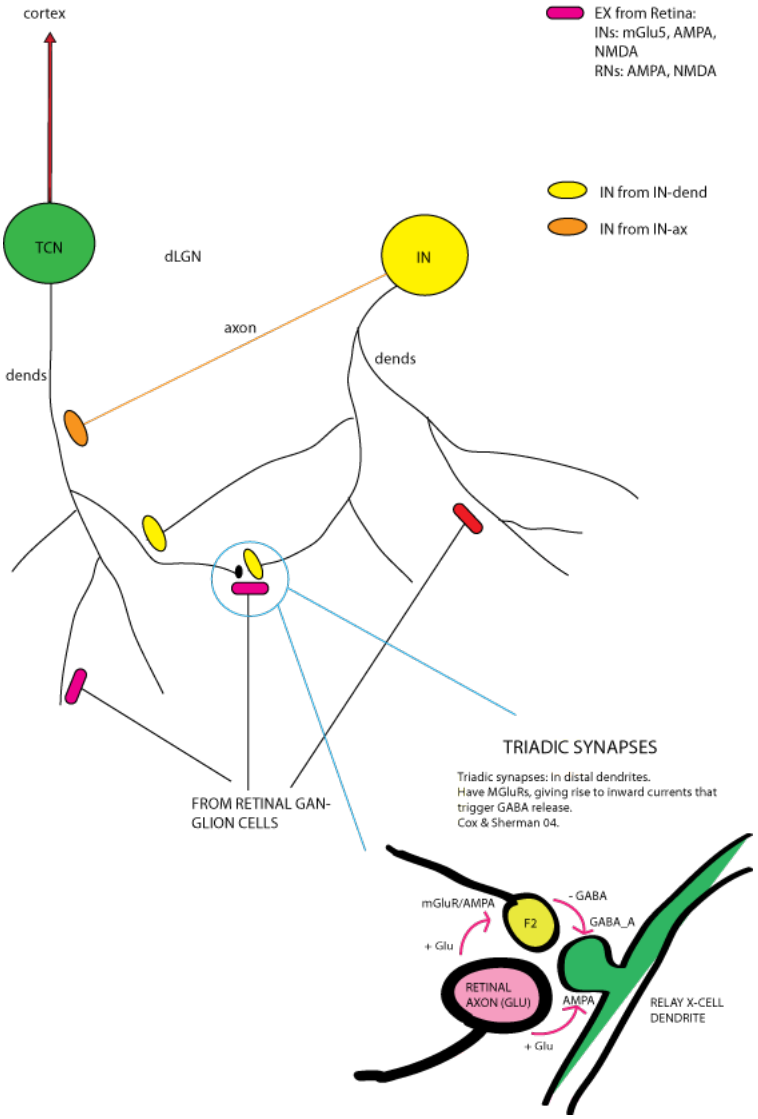

Figure 2.4: Triadic synapses between INs and TCNs. . Image made by Geir Halnes.

The conditions that are required for these sites to release GABA are unclear, and we are far from having a complete understanding of the function of INs. However, an understanding of the propagation of somatic input to the distal dendrites, and of synaptic input to the soma, seems to be an important part of understanding the INs. The focus of this thesis is on one mechanism that may play a role for this propagation: the T-type calcium channels.

2.2.3 T-type calcium channels in INs

INs can like most neurons fire stereotypical APs. Under certain conditions, INs can be found to fire bursts of APs [12]. In several studies, the conclusion is reached that there are additional mechanisms behind these bursts [12], [9].

Distribution of T-type calcium channels in INs

The distribution of I_T-channels on the somatodendritic membrane is believed to be greatly important for neuronal functioning [10]. As an example, Zomorrodi et al. [18] found in their modeling studies that of TCNs that certain distributions were optimal for the ability of TCNs to generate bursts dependent on I_T-channel.

Contradictory experimental conclusions have been reached about the distribution of I_T-channels in the IN's somatodendritic membrane. In example, Parajuli et al. [15] carried through studies based on genetic markers, finding an indication of the density of I_T-channels to be linearly increasing from soma, while the physiological studies of Munsch et al. [21] indicated I_T-channels to be uniformly distributed.

The modeling study of Halnes et al. showed that similar firing patterns could be obtained by both a uniform and a linearly increasing distributions. In this thesis, I would like to investigate whether the I_T-channel distribution is likely to strongly influence the propagation of electrical signals between the soma and the distal dendrites and the local calcium levels at specific dendritic sites.

Chapter 3

Computational Background

3.1 Cable modeling

Unless otherwise stated, everything in this chapter is based on theory from the book "Methods in Neuronal Modeling - From Ions to Networks" by Christof Koch and Idan Segev [14].

In the late 1950s a necessity arose for interpreting neuronal experimental data, causing for the application of cable theory to dendritic neurons.
Cable analysis relates for the most part to passive dendrites, where the membrane parameters are time and voltage independent. While dendrites in reality don't have this feature, cable theory is still immensely helpful in understanding excitable dendrites and their integrative mechanisms.

Neuronal axons and dendrites can be idealized as cylinders as they are made up of thin tubes of nerve membrane:

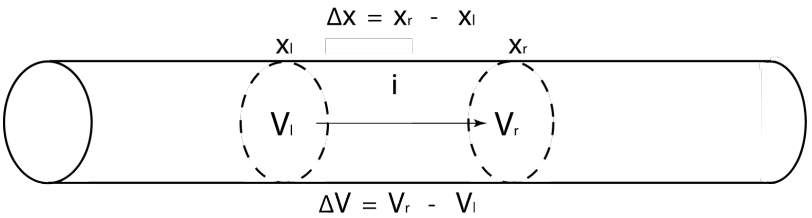

Figure 3.1: Diagram of a core cylinder, illustrating the internal current flow along core resistance, with focus on the length increment Δx and the corresponding increment in intracellular voltage. Image redrawn from [14]

Consider a length increment, Δx, of the cylinder and ΔV, the corresponding increment in intracellular voltage. Internal current flow is taken to be positive when flowing from left to right, which here also is defined as the positive x direction. Assume that the cylinder's length is several times its diameter, and that it has uniform capacitance, resistivity and electromotive force (uniform membrane properties) and also a uniform intracellular resistance per unit length, r. Viewing the cylinder as a core conductor, we

can use Ohm's law to express ΔV in terms of intracellular resistance and intracellular current

$$\Delta V = -ir\Delta x \tag{3.1}$$

Taking the limit of $\Delta V/\Delta x$ as Δx approaches zero gives

$$\frac{\partial V}{\partial x} = -ir \tag{3.2}$$

the intracellular potential gradient. Since r is constant and independent of x, the equation above can be differentiated to obtain

$$\frac{\partial^2 V}{\partial x^2} = -r\frac{\partial i}{\partial x} \tag{3.3}$$

View the cylinder segment as a node where i_l is the current flowing into the node, and i_r and $i_m\Delta x$ are the currents with outward flow.

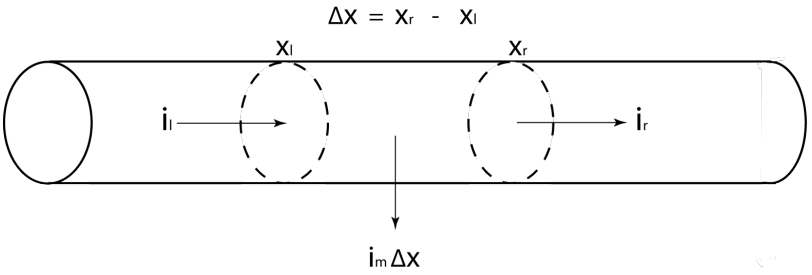

Figure 3.2: Diagram of a core cylinder, illustrating the relation of membrane current density to change in core current. Image redrawn from [14]

Since the net current flow through the node must equal zero (Kirchhoff's current law), the membrane current can be expressed

$$i_m\Delta x = i_l - i_r = -\Delta i \tag{3.4}$$

An expression for the *membrane current density* per unit length of cylinder can thus be obtained by dividing by Δx and taking the limit of $\Delta i/\Delta x$ as Δx goes to zero

$$i_m = \frac{\partial i}{\partial x} \tag{3.5}$$

Combining 3.3 and 3.5, and multiplying both sides by r_m, the membrane resistance, gives

$$\frac{r_m}{r}\frac{\partial^2 V}{\partial x^2} = i_m r_m \tag{3.6}$$

Note that V in the equations above is the internal potential. Instead let $V = V_i - V_e$, where V_i is the internal potential and V_e the extracellular potential. V_e is assumed to be independent of x and t and will be zero terms when differentiating V.

View the cylinder as an equivalent circuit where the membrane conductance lies in series with a battery (the resting potential).

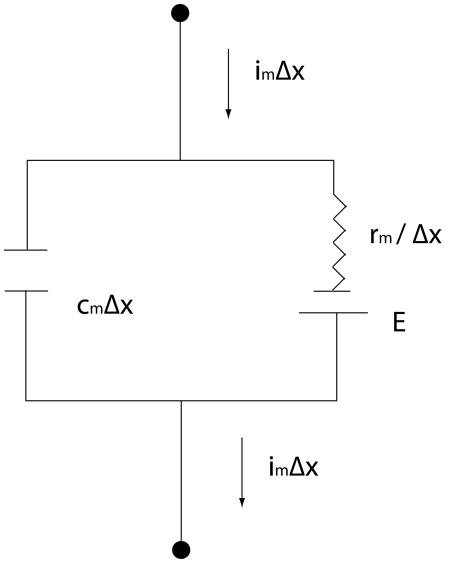

Figure 3.3: A circuit diagram showing the equivalent electric circuit for a membrane. Image redrawn from [14]

Since the membrane cylinder is passive, it has a membrane capacitance per unit length that can be expressed $c_m = C_m \pi d$ (F/cm). In parallel with this membrane capacitance is a membrane conductance per unit length, $g_m = G_m \pi d$ (S/cm). Thus, the membrane resistance is the reciprocal $r_m = 1/g_m = R_m/\pi d$ (Ωcm).
We can write i_m as a sum of conductive and capacitive currents

$$i_m = c_m \frac{\partial V}{\partial t} + \frac{V}{r_m} \tag{3.7}$$

and with $V = V_i - V_e$, we get

$$i_m = c_m \frac{\partial (V_i - V_e)}{\partial t} + \frac{V_i - V_e}{r_m} \tag{3.8}$$

Letting $V = V_m$ gives

$$i_m = c_m \frac{\partial (V_m)}{\partial t} + \frac{V_m}{r_m} \tag{3.9}$$

3.2 Ion channels

Unless otherwise stated, everything in this chapter is based on theory from the book "Dynamical Systems in Neuroscience - The Geometry of Excitability and Bursting" by

Eugene M. Izhikevich [11].

In the previous chapter, the membrane current i_m was derived for a passive membrane. i_m consists of a capacitive current $c_m \frac{\partial V}{\partial t}$ and a conductive current $\frac{V_i - V_e}{r_m}$. These properties are passive, and neuronal membranes contain additional features like several different species of ion channels. These ion channels play an important role when it comes to the firing properties of the neuron. As they open or close in a manner dependent on the activity of the neuron, they are called active mechanisms. To include the active mechanisms, the membrane current can be expressed

$$i_m = c_m \frac{\partial (V_m)}{\partial t} + \frac{V_m}{r_m} + \text{active currents} \tag{3.10}$$

An important physiological feature of neurons is the assortment of ion channels that span the membrane. Voltage changes and both internal and external signals cause the ion channels to open and close, allowing ions, mainly potassium (K^+), calcium (Ca^{2+}), chloride (Cl^-) and sodium (Na^+), to travel into and out of the cell. These ionic currents are what sustain and propagate electrical neuronal activity.

An open ion channel is permeable for specific ion types, and the opening and closing of an ion may be determined by many different signals. Most commonly, these mechanisms are voltage dependent. The focus of this thesis will be on three types of ion channels: a sodium channel, a potassium channel and a calcium channel. The theory needed to model these three channels is introduced in the sections below.

3.2.1 Hodgkin Huxley formalism

In the 1950s, Alan Lloyd Hodgkin and Andrew Huxley developed a model describing the underlying mechanisms of how action potentials are generated in neuron. Their model was based on experiments on giant axons of squid, and found three types of currents describes as the voltage-gated transient Na^+ current I_{Na}, the voltage-gated persistent K^+ current I_K and I_L, the Ohmic leak current (composed mostly of Cl-ions). These currents can be described

$$I_{Na} = \bar{g}_{Na} m^3 h (V_m - E_{Na}) \tag{3.11}$$

$$I_K = \bar{g}_K n^4 (V_m - E_K) \tag{3.12}$$

$$I_L = g_L (V_m - E_L) \tag{3.13}$$

where g_{Na}, g_K and g_L are the maximum conductances for the channels when they are fully open. The gating variables n, m and h (n is the K^+ activation variable, m is the Na^+ activation variable and h is the Na^+ inactivation variable) determine the probability of a channel being in the open state (for a many channels, the variables tell the fractions of channels that are open). E_{Na}, E_K and E_L are the reversal potentials for each specific ion type.

The Hodgkin-Huxley model was developed specifically for the giant squid axon, but many of the other ion channels in the brain can be modeled using this formalism which has come to be known as the Hodgkin-Huxley formalism.

Equilibrium potential

Concentration and electric potential gradients are the main forces that drive ions across the membrane channel. Ions will diffuse down the concentration gradient (i.e. from higher concentration outside cell to lower concentration inside), causing charge to accumulate on opposite sides of the membrane surface. This creates a potential gradient across the membrane (transmembrane potential), which in turn leads to slowing down of the diffusion. Eventually *equilibrium potential* is reached, where the electrical potential gradient and the concentration gradient counterbalance each other by exerting equal and opposite forces, resulting in zero net current across the membrane. Equilibrium potential can be expressed by the Nernst equation

$$E_{ion} = \frac{RT}{zF} \ln \frac{[Ion]_{out}}{[Ion]_{in}} \tag{3.14}$$

where R is the universal gas constant, T is temperature given in degrees Kelvin, z is the valence of the ion and F is Faraday's constant. $[Ion]_{out}$ and $[Ion]_{in}$ denote the ionic concentrations outside and inside the cell.

When the membrane potential doesn't equal the equilibrium potential, there will be a net ionic current, I_{ion}, that is proportional to the difference between the potentials.

Voltage gates

Each ion channel has gates that control their electrical conductance by switching the state of the channel between open and closed states. For an individual channel, the alteration between open and closed states will be of stochastic nature, but for a large enough population of identical channels the net current generated can be written as

$$I = \bar{g}p(V - E) \tag{3.15}$$

where $\bar{g}$ is the population's *maximal conductance* and p is the proportion of channels that are in the open state (in average).

The gates may act in response to neurotransmitters and neuromodulators (e.g NMDA, AMPA, or GABA receptors), they may be influenced by second messengers (e.g. Ca^{2+}-gated K^+ channels), or they may be sensitve to membrane potential (e.g. voltage-gated K^+ and Na^+ channels). Voltage gates are either *active* or *inactive* - they either open or close channels. In a large population, the proportion of open channels can be written

$$p = m^a h^b \tag{3.16}$$

where m is the probability of an activation gate being in open state, a is the number of activation gates per channel, h is the probability of an inactivation gate being in open stat and b is the number of inactivation gates per channel. The channels are *partially activated* if $0 < m < 1$, *completely activated* if $m = 1$, *deactivated* (not activated) if $m = 0$, *inactivated* if $h = 0$ and *deinactivated* (not inactivated) if $h = 1$. A channel with inactivation gates has *transient* currents, while if the channel doesn't have inactivation gates, the current through the channel will be *persistent* and $p = m^a$.

A first-order differential equation can describe the dynamics of m, the activation variable

$$\dot{m} = (m_\infty(V) - m)/\tau(V) \tag{3.17}$$

Here $m_\infty(V)$ is the *steady-state activation function*, and $\tau(V)$ is the *time constant*. Both can be measured experimentally.
Similarly, the dynamics of the inactivation variable h can be described

$$\dot{h} = (h_\infty(V) - h)/\tau(V) \tag{3.18}$$

where $h_\infty(V)$ is the *steady-state inactivation function*.

The activation and inactivation variables from equations 3.11 to 3.13 have opening and closing dynamics that can be described by the following equations

$$\begin{aligned} \dot{n} &= (n_\infty(V) - n)/\tau_n(V) \\ \dot{m} &= (m_\infty(V) - m)/\tau_m(V) \\ \dot{h} &= (h_\infty(V) - h)/\tau_h(V) \end{aligned} \tag{3.19}$$

$n_\infty(V)$, $m_\infty(V)$ and $h_\infty(V)$ are the steady-state activation functions, and $\tau_n(V)$, $\tau_m(V$ and $\tau_h(V)$ are the voltage-dependent time constants. These are typically found in empirical studies, and vary between ion channels. They also vary between different neurons.

The following figure shows examples of the dynamics of the above functions. Note the normalization of the y-axis such that 1 denotes all channels being open.

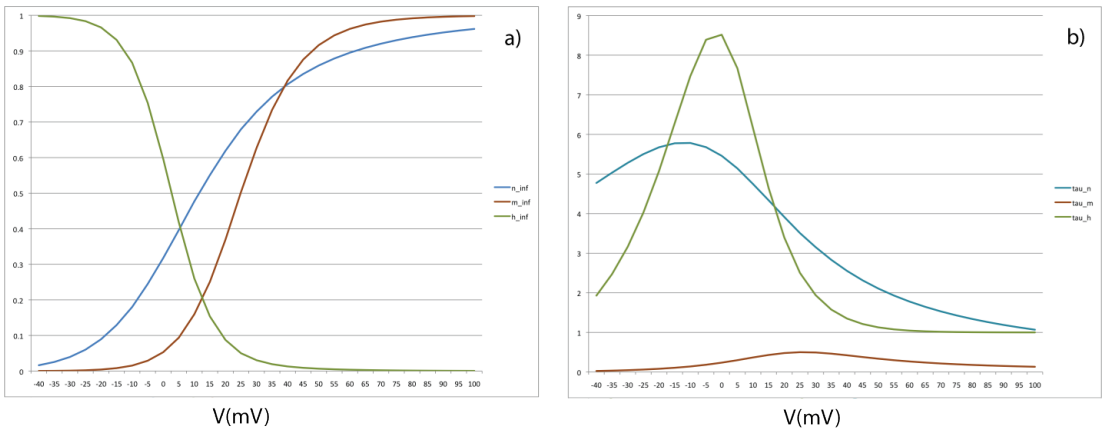

Figure 3.4: **a**) Dynamics of the steady-state activation and inactivation functions **b**) Dynamics of the voltage-dependent time constants.

3.2.2 GHK formalism

Another formalism for describing the dynamics of gated ion channels is the Goldman-Hodgkin-Katz (GHK) formalism. It is related to the Hodgkin Huxley formalism, and

does not have a constant reversal potential.

The intracellular calcium concentration for a neuron at rest is very low, and an incoming flux of Ca^{2+} ions will likely significantly alter the concentration. One can therefor not assume the reversal potential to be approximately constant, and the GHK formalism therefore comes in handy.

The calcium current can be expressed [3]:

$$I_T = \bar{P}_{Ca} m^2 h G(V, Ca_o, Ca_i) \tag{3.20}$$

where $\bar{P}_{Ca}$ is the membranes maximum permeability of Ca^{2+} ions (cm/s), and Ca_o and Ca_i represent the intracellular and extracellular calcium concentrations. $G(V, Ca_o, Ca_i)$ is a nonlinear function expressing the voltage and ionic concentrations:

$$G(V, Ca_o, Ca_i) = Z^2 F^2 V/RT \frac{Ca_i - Ca_o \exp(-ZFV/RT)}{1 - \exp(-ZFV/RT)} \tag{3.21}$$

Here Z is the valence of calcium ions (Z=2), F is Faraday's constant, R is the gas constant and T is the temperature in Kelvins.

The function for the voltage and ionic concentrations has dimension mC/cm^3, and must therefore be multiplied with a permeability (cm/s) to obtain the units mA/cm^2 for the I_T current. This is equivalent with the multiplication of conductance in the Hodgkin-Huxley formalism. The permeability is proportional to the conductance, and both are related to the ion channel density.

The gating variables m and h (see equation 3.19) are modeled as they are in the Hodgkin Huxley formalism.

3.2.3 Intracellular calcium concentration

A model that accounts for the variations in intracellular calcium concentration must include an algorithm for computing the concentration changes as a function of time. An extrusion mechanism of the following form is the most simple model [9]:

$$\frac{d[Ca]}{dt} = -\alpha \cdot I_{Ca} - \frac{[Ca] - [Ca]_{rest}}{\tau_{Ca}} \tag{3.22}$$

$[Ca]$ is the intracellular calcium concentration, $[Ca]_{rest}$ is the calcium concentration at rest, and the calcium current I_{Ca} may consist of a current through several calcium channels.

3.3 Compartmental neural models

3.3.1 Principles of compartmental neuron models

Detailed information about interactions between synaptic input, morphology and physiological properties is necessary in order to properly understand how information is processed in each neuron. A good approach to exploration of deviations in voltage, flow of current and the effect of and relations between different input and output is to create a formal, *compartmental model*, that encompasses these features. In this model one assumes that small neuronal segments can be treated as having uniform potential, such that one can approximate the continuos structure of the neuron as a series of discrete linked elements. Doing this will make the mathematics simpler, and also allow for an individual compartment to have nonuniform properties.
In this chapter a description of compartmental modeling will be given, based on theory from the book "Methods in Neuronal Modeling - From Ions to Networks" by Christof Koch and Idan Segev [14]. This theory is incorporated when one builds compartmental neural models.

Recall equation 3.9:

$$i_m = c_m \frac{\partial V_m}{\partial t} + \frac{V_m}{r_m}$$

Multiplying both sides by r_m and collecting terms leads us to

$$i_m r_m - c_m r_m \frac{\partial V_m}{\partial t} - V_m = 0 \tag{3.23}$$

Recall equation 3.6:

$$\frac{r_m}{r} \frac{\partial^2 V}{\partial x^2} = i_m r_m$$

Inserting this equation gives

$$\frac{r_m}{r} \frac{\partial^2 V_m}{\partial x^2} - c_m r_m \frac{\partial V_m}{\partial t} - V_m = 0 \tag{3.24}$$

a partial differential equation in a form used in one-dimensional cable theory to describe the flow of current in a continuous passive dendritic tree.

For transient current inputs in an idealized class of unbranched dendritic tree, these equations have simple analytical solutions. However, too many constraints are made in achieving this idealization, and the model far from resembles a real dendritic tree.

When considering arbitrary branching passive dendritic trees, the solutions to the cable equations (3.24) become more complex, and if, additionally, the neuron's membrane properties are voltage dependent, one cannot implement the analytical model. The linear cable theory is no longer valid, and compartmental models must be used to deal with these more complex cases.

In compartmental models, the neuron is divided into segments each assumed to be isopotential, and the continuous neuron can thus be approximated as discrete elements

linked together. The continuous differential equations of the analytical model are replaced by a set of ordinary differential equations, with an error that will be negligible if the neuron is divided into sufficiently small segments. An equivalent circuit is used to represent the neuron segments if one assumes the membrane to be passive. Each membrane channel can be represented as a resistor ($\hat{r}_{m_j}$) connected in parallel with a capacitor ($\hat{c}_{m_j}$), and series resistances (r_j) representing the cytoplasm connect neighboring compartments. The extracellular environment is taken as reference potential (ground). Figure 3.5 illustrates the representation of neuron segments as an equivalent circuit.

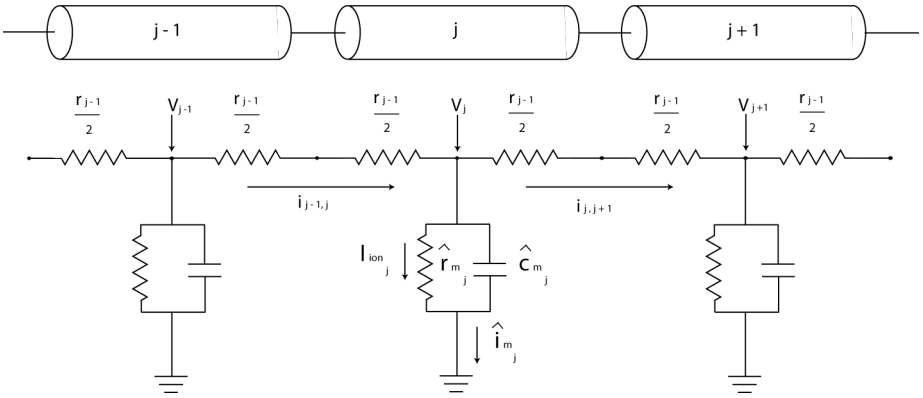

Figure 3.5: Equivalent circuit for a compartmental model of a chain of three successive small cylindrical segments of passive dendritic membrane. Image redrawn from [14].

An advantage of the above approach is that each compartment is not restricted and may assume either somatic, axonal or dendritic membrane properties. Another advantage is that compartmental models allow for different levels of resolution- neurons can soundly, as is the case with this thesis, be represented with a few compartments, each comprised of complex structures.

3.3.2 A mathematical representation

Kirchhoff's current law states that the net current flow through a node in an electrical circuit will be zero. Each equation in the system of ordinary differential equations used to describe compartmental models is derived from Kirchhoff's law, so in each compartment, j, the difference between the current entering ($i_{j-1,j}$), and the current leaving ($i_{j,j+1}$) will equal the net current through the membrane ($\hat{i}_{m_j}$) which in an unbranched section can be expressed

$$\hat{i}_{m_j} = i_{j-1,j} - i_{j,j+1} \tag{3.25}$$

Analogy to the equivalent circuit allows us to represent the membrane current as a sum of a current due to various ion channels (I^{ion}) and a current due to the membranes capacitative properties

$$\hat{i}_{m_j} = \hat{c}_{m_j} \frac{dV_j}{dt} + I_j^{ion} \tag{3.26}$$

where V_j is the membrane potential. An additional term (I^{stim}) must be added to account for stimulation that the compartment may receive from an external source, or as synaptic

input from other neurons. Expressing $i_{j-1,j}$ and $i_{j,j+1}$ as the voltage gradient between compartments divided by the axial resistance between them gives

$$\frac{V_{j-1} - V_j}{r_{j-1,j}} + \frac{V_j - V_{j+1}}{r_{j+1,j}} = \hat{c}_{m_j} \frac{dV_j}{dt} + I_j^{ion} + I_j^{stim} \tag{3.27}$$

or

$$(V_{j-1} - V_j) g_{j-1,j} - (V_j - V_{j+1}) g_{j,j+1} = \hat{c}_{m_j} \frac{dV_j}{dt} + I_j^{ion} + I_j^{stim} \tag{3.28}$$

where the axial resistance is expressed in terms of conductance.

3.4 NEURON simulator

NEURON is a simulation program developed by John W. Moore and Michael Hines at the Department of Neurobiology at Duke University. It provides an environment for modeling and simulating neuronal networks, and enables us to tackle problems that are closely linked to experimental data. Complex models are built by connecting one-dimensional sections together to form arbitrary neuron morphologies in which we can insert membrane properties (i.e. ion channels, capacitance, synapses) [17].

The default graphic interface (GUI) of NEURON is designed to hide the numerical methods used in simulation, thus providing an intuitive environment where users can combine the GUI and hoc programming to generate results. By offering a syntax where model properties can be specified in familiar idioms, users are allowed to focus on addressing biological questions without being distracted by low-level mathematical or computational issues (i.e. introducing the notion of a *section* as an analogy to an unbranched neurite so that users can work with the anatomy of neurons without having to deal with the cable equation) [17].

An extendable library of biophysical mechanisms is available, through which user-defined mechanisms (i.e. diffusion, voltage-gated channels) can be added by writing model descriptions in the programming language NMODL that has syntax with which kinetic schemes and sets of simultaneous equations can be expressed [17].

3.4.1 Creating the compartmental model using the NEURON simulator

Following is a short overview of the principles surrounding the creation of a compartmental model.

On the onset of creating a compartmental model, the structure of real neurons are mapped by reconstructing them into series of linked, discrete geometric segments. The dimension of each segment is measured, and it's physical location in space is represented in this reconstruction that may be carried out using methods like light microscopy [14].

Neurolucida is a software system for brain mapping that produces 3D reconstructions of neurons [16]. These mappings can be read by NEURON. Neurolucida files are

often used when dealing with realistic morphologies, and the compartmentalization of these morphologies is handled automatically by NEURON algorithms.

Available online are NMODL-based files that describe the kinetics of ion channels, and of the intracellular calcium concentration. These files are often adapted to experimental recordings made for the given ion channel in a specific cell.

A HOC-file then needs to be set up, specifying how many segments the model is to be divided into, the passive membrane properties of the model neuron and the set of ion channels to be inserted into each segment of the model.
To validate the model, the responses of simulations are compared to experimental recordings of the same type of cell, and adaptation of experimental data can be carried through by varying unknown parameters. As the ion channel densities may vary in reality, the parameters one is free to vary are often the different ion channel conductances, and the ion channel distribution over the membrane. The ion channel kinetics is typically known, and thus usually remains unvaried.

Chapter 4

Methods

In the compartmental model of the LGN interneuron, the following values and properties need were specified: a morphology, passive membrane properties, kinetics that are included in the model, an algorithm for computing the intracellular concentrations of a given ion, and the distribution of ion channels throughout the membrane of the soma and dendrites.

In my simulations, a simplified version of a previous model for dLGN interneurons was used [9]. In this previous model created by Halnes et al. a morphological reconstruction of interneurons was used to create a compartmental model that is able to reproduce and account for key features of experimental recordings. The same morphology was used here.
Of the two parameterizations in the Halnes et al. model, I use the one called P2.
As this study focused on the effects of various distributions of T-type calcium channels, I only included the following 3 channels to the simplified model: the Hodgkin-Huxley sodium channel (Na) and the delayed-rectifier potassium channel (K_{dr}) that are responsible for generation of action potential, and low-threshold, T-type calcium channels (I_T), that underlie bursts and T-type calcium spikes [13], [9] .

For the simplified model, the morphology, passive membrane properties (with one adjustment, see chapter 4.1.2), ion channel kinetics, and algorithm for the intracellular calcium pool are taken from the Halnes et al. model. These shared properties are described in chapter 4.1.
Variations were only made to the densities and distributions of the included ion channels, and to the reversal potential for the passive currents, properties that will be described in chapter 4.2. Finally, chapter 4.4 gives a description of the simulation setup.

4.1 The reduced Halnes et al. model

4.1.1 Morphology

In the model used by Halnes et al., a 3D reconstruction of mouse interneurons was created based on the morphology shown in the figure below

Figure 4.1: The dLGN interneuron morhpology that was used in all simulations.

This shows an image of an interneuron drawn using Neurolucida neuron reconstruction software following experiments on brain slices containing dLGN of knock-in-mice. The interneuron model consists of a soma and 104 dendritic sections split into 330 segments, and has the following parameters: total surface area = 9864 μm^2, total length of dendrites = 5771 μm (with longest dendrite = 673 μm), mean somatodendritic diameter 0.5 μm (approximately). The model does not contain any axons as they in LGN interneurons tend to be very thin and difficult to identify in the morphology data. This omission of axons is not crucial as they, due to small surface area, do not have a significant effect on somatic input- and output-data.

4.1.2 Passive properties

The following passive properties are the same as used by Halnes et al. (see table 4.1 for an overview): axial resistivity $R_a = 113\ \Omega cm$, membrane capacitance $C_m = 1.1\ \mu F/cm^2$, membrane resistance $R_m = 45\ k\Omega cm^2$, leakage current $g_{pas} = 1/R_m$. In order to obtain a qualitative fit of responses to current injections in the soma, with the exception of R_a, they manually estimated these properties for the neuron through a trial and error process.
The reversal potential was initially set to the same value as Halnes et al. ($E_{pas} = -71.6\ mV$), but slightly altered to $-71\ mV$ after a series of adjustments were made to the ion channel conductances, in order to recover a resting potential of $\sim -69\ mV$, which was the resting potential of the neuron P2 in Halnes et al. The resulting resting potential was $V_{rest} = -69.4\ mV$.

Table 4.1: Passive parameters

Parameter	Description	Value
V_{rest}	Resting potential	$-69.4\ mV$
R_m	Membrane resistance	$45000\ \Omega cm^2$
C_m	Membrane capacitance	$1.1\ \mu F/cm^2$
R_a	Axial resisitivty	$113\ \Omega cm$
E_{pas}	Reversal potential	$71\ mV$

4.1.3 Ion channel kinetics

I_T

Halnes et al. adapted the kinetics of the low-threshold T-type calcium channel (I_T) from interneuron voltage clamp data. The I_T-channel kinetics was taken from Halnes et al., where it had been adapted to voltage clamp and current clamp data from INs. A Goldman-Hodgkin-Katz formulation can be used to describe the I_T current (see section 3.2.2)

$$I_T = \bar{P}_{Ca} m^2 h G(V, Ca_o, Ca_i) \tag{4.1}$$

Na **and** K_{dr}

The Na and K_{dr} channels were also taken directly from Halnes et al., who found that these were appropriate for modeling the APs of INs. A Hodgkin-Huxley formulation as described in chapter 3.2.1 can be used for Na and K_{dr} channels, and the currents can be described

$$I_{Na} = g \cdot m^3 \cdot h \cdot (V - E_{Na}) \tag{4.2}$$

and

$$I_K = g \cdot n^4 \cdot (V - E_K) \tag{4.3}$$

The image below shows the kinetics of the ion channels described above

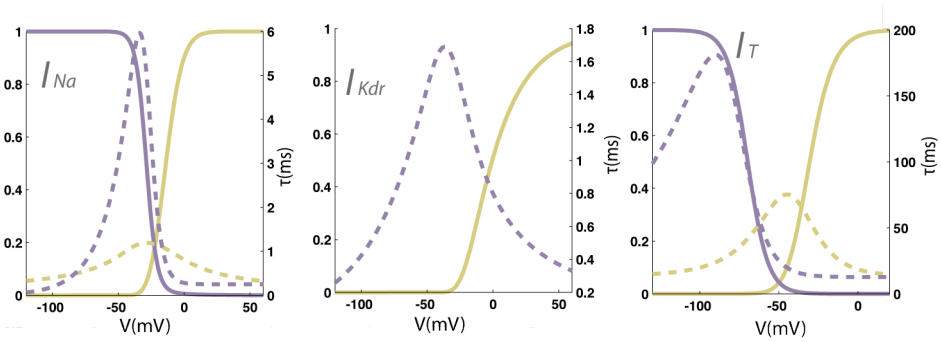

Figure 4.2: The steady state values of activation/inactivation variables (purple/yellow full lines), along with the activation/inactivation time constants (dotted lines) plotted as a function of voltage for the Na, K_{dr} and Ca ion channels. Image from Halnes et al. [9]

4.1.4 Calcium pool

When modeling the intracellular calcium levels, I used the model of a leaky integrator, expressing the calcium concentration as

$$\frac{d[Ca]}{dt} = -\alpha \cdot (I_T) - \frac{[Ca] - [Ca]_{rest}}{\tau_{Ca}} \tag{4.4}$$

Increase in calcium concentration when the calcium channels are open was modeled by the first term on the right hand side, where the factor $\alpha = 0.0155\ mmol/(cm \cdot C)$ converts the I_T current into a concentration increase. The second term helped describe buffering and extrusion mechanisms, with the values $[Ca]_{rest} = 50nM$ and $\tau_{Ca} = 50\ ms$. The calcium extrusion mechanism and all parameters were taken directly from Halnes et al.

4.2 Model parameters that were varied

The following model parameters were changed with respect to the Halnes et al. model: E_{pas}, g_{Na}, $g_{K_{dr}}$ and g_T. These parameters were specified so that the IN model responded in a realistic way to selected inputs (see results). In all simulations, the values $E_{pas} = 71mV$, $g_{Na} = 0.08S/cm^2$ and $g_{K_{dr}} = 0.3S/cm^2$ were used, with the same distribution of g_{Na} and $g_{K_{dr}}$ as in Halnes et al., that were assumed to be uniform across the dendrite, and not equal to the distribution in the soma.

4.2.1 T-cannel distributions

Simulations were carried through using four different ion channel distributions that are described below.
When varying the ion channel distributions, the total number of I_T-channels was kept

constant. The values of g_{soma} are therefore individual for each distribution.
A functional form is used to express the channel distribution, where g_{soma} is the reference point. In this way g_{dend} is entirely specified by g_{soma} and the chosen distribution.

Linearly increasing distribution

The first distribution, $g_{T_{lin}}$ is the same as that used by Halnes et al. where the dendritic density g_{dend} increases linearly with distance x (μm) from soma by the formula $g_{dend}(x) = g_{soma} \cdot (1 + 0.04x)$.

Uniform distribution

In the second distribution, $g_{T_{lin}}$, the dendritic density is uniform and equal to the distribution in soma: $g_{dend}(x) = g_{soma}$.

Zero distribution

The third distribution used is one where all the I_T channels were located in the soma, and $g_{dend} = 0$. This distribution is denoted $g_{T_{null}}$.

Zomorrodi distribution

The stepwise form of the fourth distribution, $g_{T_{Zom}}$, is based on the experiments of Zomoroddi et al. [18] in which they investigated different patterns of I_T-channel distributions in thalamocortical cells.

I chose one of these was chosen as a starting point for the experiments in this thesis.

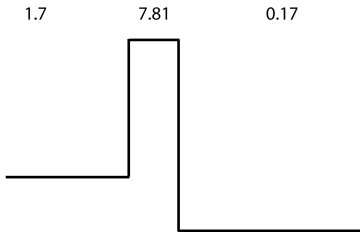

Figure 4.3: Her skal det vaere bilde av Zomorrodifordelningen

The image above shows the permeability ($x10^4$ cm/s) of the I_T-channel distribution.

First, I determined the length of the specific dendritic pathway of which the propagating signal was to be studied (this needed to be done for each new pathway) and divided into three segments. The length of these segments was determined by the relative lengths in the Zomorrodi 3-compartment-model. Due to the proportionality between the conductance and permeability, these segments could be assigned with the densities $g^1_{dend} = g_{soma} \cdot 1.7$, $g^2_{dend} = g_{soma} \cdot 7.81$ and $g^3_{dend} = g_{soma} \cdot 0.17$.
g^1_{dend} was defined as all segments between soma (distance = 0 μm) and 201 μm, g^2_{dend} the segments with distance 202 μm to 303 μm and g^3_{dend} the segments with distance

304 μm to 672 μm (the tip of the dendrite). These values were set globally for the entire neuron, which didn't matter as the focus was only on the chosen pathway.

4.2.2 Normalization of gT

The total number of I_T channels was held equal through all experiments. This was in order to enable comparison of documented differences in the signals resulting from inputs *i-iv*. To assure the constancy of the number of channels, g_{soma} was varied for each distribution of I_T-channels such that the sum $(A_{soma} \cdot g_{soma}) + (\sum_i A_i \cdot g_{dend_i}(x))$ remained constant. Here A_i is the cross section area of dendritic segment i, and g_{dend} for each distribution is given by the formulas in section 4.2.1.

Gathered in the table below are the values of the various conductances.

Table 4.2: Maximum conductances

Parameter	Description	Value
g_{Na}	Maximum Na-conductance in soma	0.08 S/cm^2
g_{Kdr}	Maximum K_{dr}-conductance in soma	$0.3 S/cm^2$
$g_{soma_{lin}}$	Maximum I_T-conductance in soma (lin. incr. dist.)	$9 \cdot 10^{-6}$ S/cm^2
$g_{soma_{uni}}$	Maximum I_T-conductance in soma (unifrom dist.)	$8.53 \cdot 10^{-5}$ S/cm^2
$g_{soma_{zero}}$	Maximum I_T-conductance in soma (zero dist.)	$1.66 \cdot 10^{-3}$ S/cm^2
$g_{soma_{Zomorrodi}}$	Maximum I_T-conductance in soma (Zomorrodi dist.)	$5.008 \cdot 10^{-5}$ S/cm^2

4.3 Modeling a synapse

Excitatory post synaptic currents (EPSCs) can be evoked by the activation of AMPA synapses. These have been measured in interneurons [5]. i modeled the AMPA current in a standard way, as a sum of two exponentials. This function is incorporated in the NEURON library. The EPSC that is evoked by the activation of a single synapse has a time course that resembles that of TCNs (this can be seen in comparing the top trace if figure 4B in Acuna-Goycolea et al [5] with the bottom trace in figure 1B in Blitz & Regehr [1]). We approximated by assuming the AMPA synapse to be similar in INs and TCNs. For the reversal potentia ($Erev = 10mV$), the rise and decay times were chosen to be, $t_{rise} = 0.5ms$ and $t_{dec} = 2ms$, values based on data in Blitz & Regehr for AMPA synapses in TCNs. The conductance was determined in our simulation (see results).

4.4 Inputs to the model

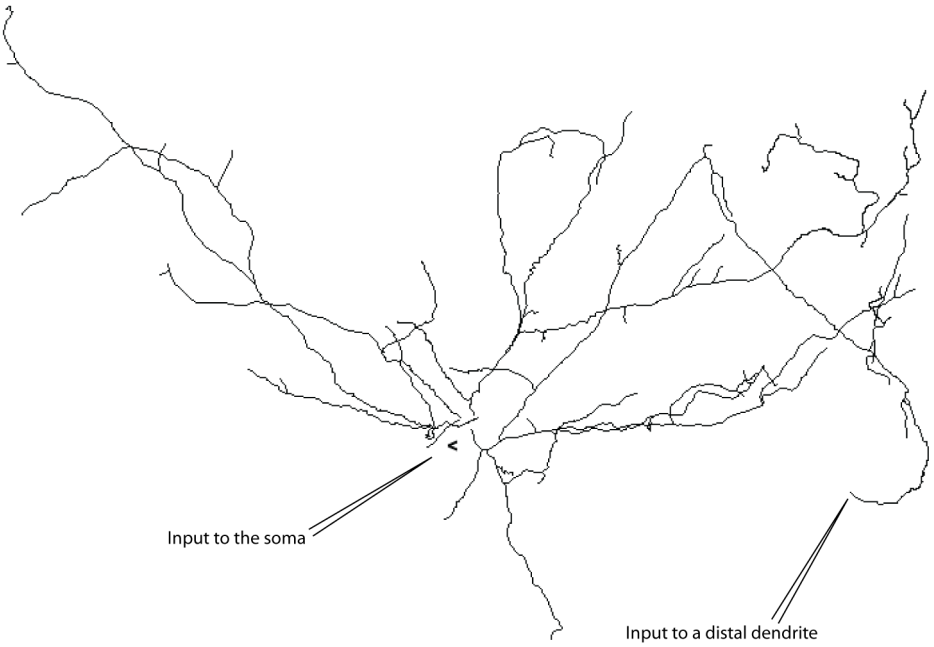

Figure 4.4: The dLGN interneuron, illustrating where inputs were made.

The model's response to the following 4 different inputs was simulated:
i: short (10 ms), strong amplitude (0.2 nA $<$ amp $<$ 0.25 nA)
ii: short (10 ms), strong amplitude (as i) + blocked Na-channels
iii: long (900 ms), low amplitude (0.03 nA $<$ amp $<$ 0.04 nA)
iv: synaptic input to the distal dendrites

When changing between the distributions and the values of g_{soma}, I found that the strength of the input signal needed to be adjusted in order for the signal to resemble those described as responses to inputs i - iv.

I varied the amplitudes of inputs i to iii, and tested different synaptic strengths. A further description is provided in the following chapter.

Chapter 5

Results

5.1 Model calibration

I wanted to see how the distributions of I_T-channels affected the model's response to the four different classes of inputs (i-v specified below). From experiments by Acuna-Goycolea et al.[5], we know that a short and strong (high amplitude) current injection to the soma will typically evoke a burst of action potentials in interneurons. We also know that a relatively long and weak somatic current injection typically evokes an initial burst that is followed by regular action potential firing [9].

Using the linear I_T-channel distribution $g_{T_{lin}}$, I set the stimulation amplitude to $0.25nA$ with duration $10ms$. At this level the response signal response was somewhat close to the wanted shape.
The values of g_{Na}, $g_{K_{dr}}$, g_{Na} and g_T were then adjusted such that the shape better resembled that of Acuna-Goycolea (mentioned above, see figure 5.1 a)). These values were held constant for the remainder of the simulations.
The response of setting $g_{Na} = 0$ was checked, showing a calcium spike. The simulation duration was then set to $900ms$, and the amplitude adjusted until a similar response as Halnes et al. was reached.

These inputs are summarized below, with the values for the linear I_T-channel distribution $g_{T_{lin}}$

Input signal i A short ($10\ ms$) and relatively strong somatic current injection was tested, varying the amplitude of the imput signal until the response signal resembled that of the signal in experiments by Acuna-Goycolea et al. [5] (where whole-cell recordings were carried out on interneurons, finding that $10ms$ current injections to the soma evoked a burst of spikes riding on a calcium spike). I found that an amplitude of 0.25 nA was suitable. The shape of this signal can be seen in figure 5.1a).

Input signal ii When setting the the sodium conductance g_{Na} to zero, input signal i still lead to a response, a "bumb" indicating the existence of an underlying calcium

spike. Figure 5.1b) illustrates this signal.

Input signal iii A long (900 *ms*) and relatively strong somatic current injection was tested, varying the amplitude of the imput signal until the response signal resembled that of the signal in the experiments of Halnes et al. I found that an amplitude of 0.0379 *nA* was suitable, and the resulting signal is shown in figure 5.1c).

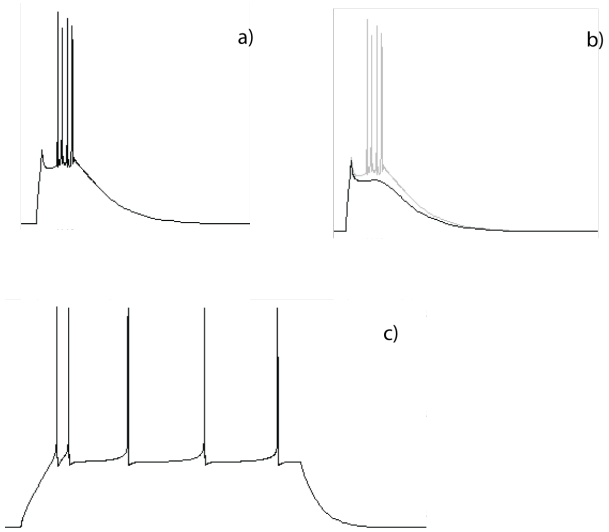

Figure 5.1: a) Response to a 10ms, 0.25nA current injection. b) Response to a 10ms 0.25nA current injection, with $g_{Na} = 0$. c) Response to a 900ms 0.0379nA current injection.

iv: synaptic inputs In addition to the input signals *i* - *iii*, I studied the effect of synaptic inputs to distal dendrites. These inputs were meant to simulate the activation of AMPA synapses leading to a brief current inflow to the neuron. See section 5.3.3 for a closer description

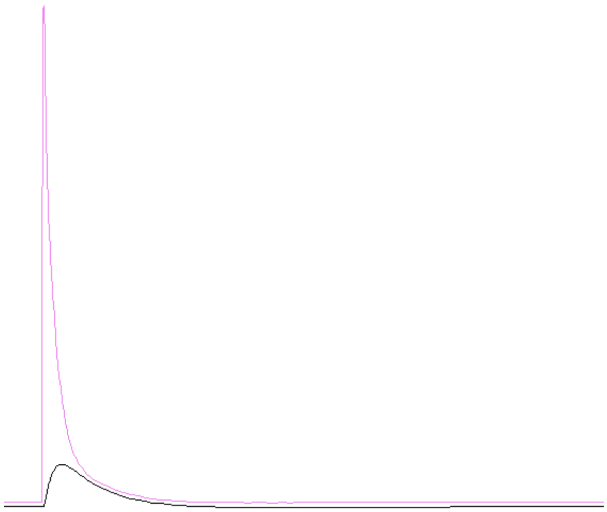

Figure 5.2: Response to subthreshold synaptic input in a distal dendrite. The black line shows the somatic response, while the purple line shows the respone in the distal denrite of which the signal was activated.

Reasonable calcium levels As the model of this thesis does not include the calcium-dependent mechanisms I_{AHP} and I_{CAN}, it was necessary to check that bursts and rapid spiking still gave rise to reasonable increases in calcium concentration. Finding that action potentials in the soma lead to concentration increases of about 75 nM in the soma, and about 700 nM in the distal dendrites, which is within the ranges found by Acuna-Goycolea et al. [5]

5.2 How the somatic response to somatic current injection depends on I_T-distributions

I also wanted to see how the somatic response to somatic current injections depended on the distribution of I_T-channels. For the remaining distributions $g_{T_{uni}}$, $g_{T_{zero}}$ and $g_{T_{Zom}}$, I checked which signal amplitude (in inputs i-iii) that was required to reproduce a similar response patterns to that in figure 5.1: for input i)- a burst with approximately the same number of spikes, and for input iii)- a burst with approximately the same number of spikes followed by approximately the same amount of regular AP firing. The following values were found (recall that g_{soma} is varied to keep the total number of I_T-channels constant):

Table 5.1: Values of g_{soma}, and signal amplitudes for I_T-channel distributions i-iii

	$g_{T_{lin}}$	$g_{T_{uni}}$	$g_{T_{zero}}$	$g_{T_{Zom}}$
g_{soma} (S/cm^2)	$9.00x10^{-6}$	$8.53x10^{-5}$	$1.66x10^{-3}$	$5.28x10^{-5}$
input i & ii (nA)	0.25	0.247	0.21	0.245
input iii (nA)	0.0379	0.0373	0.037	0.0374

The variation in input signal i) and ii) is of $\sim$ 16%, while it is of $\sim$ 2% for input iii). These values were kept for the remainder of the simulations.
(Note that as these input signal amplitudes only result in *similar* and not *identical* responses, a comparison of the different I_T-channel distributions with respect to these amplitudes would not be useful. They were only found for the purpose of setting values to be used in the following simulations.)

5.3 Signal propagation in the dendrite depends on I_T-distribution

An initial hypothesis was that the distribution of I_T-channels may be more important for signal propagation in the dendrites than for somatic responses to somatic current injections. Therefore, I wanted to compare how the propagation of the following signals (see figure 5.1) depended on the distribution of I_T-channels:
i) A burst evoked in the soma
ii) A calcium spike evoked in the soma
iii) A single action potential evoked in the soma
I also wanted to investigate how
iv) An excitatory post synaptic potential (EPSP) propagated towards the soma when a synaptic input was given to the distal dendrite (see figure 5.2).

Figure 5.3 illustrates how the signals propagated. It is plotted for the soma (black), a midway location ($x = 251\mu m$ purple) and a distal location ($x = 602\mu m$, brown).

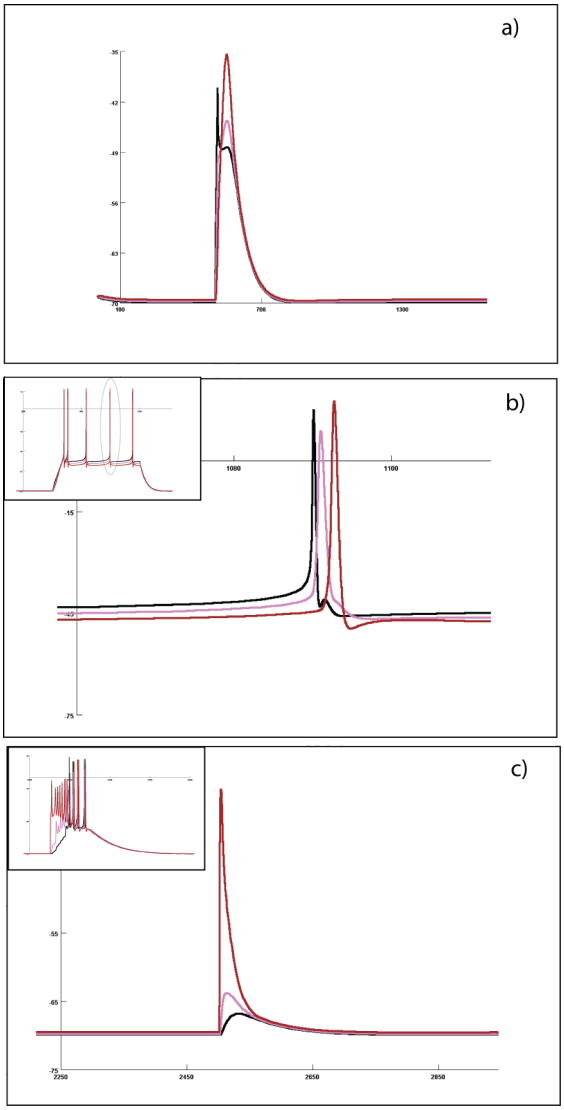

Figure 5.3: **a**) Propagation of a calcium spike (input ii) **b**) Propagation of an action potential (input iii) **c**) Propagation of a a EPSP (input iv). The inlay shows a signal above threshold.

Investigations were carried out on the four different distributions of I_T-channels, and the results were compared.
When evoking the somatic responses i-iii, I used the input amplitudes in table 5.1. These are dependent on the distribution of I_T-channels and ensure a similar somatic response in the four different distributions, hence making a good reference point for comparison.

i For i) I selected the second last spike in the burst (see figure 5.1 a)), and followed its propagation down the dendrite, recording the amplitude and width of this action potential at different points in the dendrite. I also recorded the maximum amplitude of the elevation in calcium levels resulting from the firing.

ii In a similar fashion for ii), the amplitude of the calcium spike that resulted from setting the conductance g_{Na} to zero (see figure 5.1 b)) was recorded.

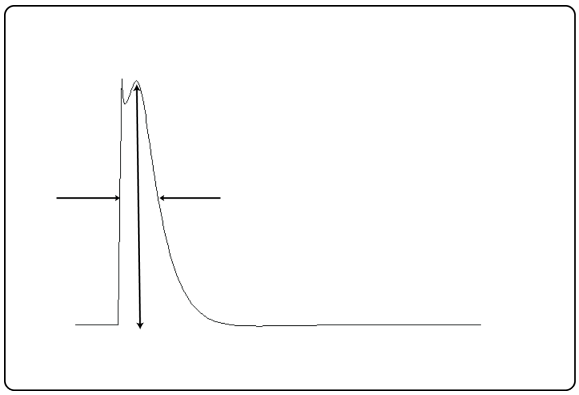

Figure 5.4: Dendritic signal respose to input ii. The arrows show that the amplitude was recorded from base to top of the calcium spike, and the width was recorded at half amplitude.

iii For iii) the amplitude of the second last spike (see figure 5.1 c)), and the resulting calcium elevation levels were recorded. The image below shows how recordings were made this input

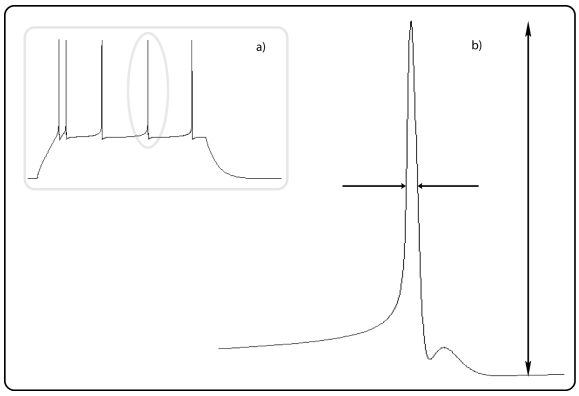

Figure 5.5: a) Somatic signal respose to input iii. The circle shows the action potential that was studied. b) Close-up of the circled action potential. The arrows show that the amplitude was recorded from base to top of the action potential, and the width was recorded at half amplitude.

iv For the synaptic input iv), I studied the response to a signal synapse placed at the tip of a single dendrite (shown in figure 4.4). The synaptic weight was set to 0.0018 μS such that the signal was below the threshold for somatic action potential firing for all distributions. All distributions were tested with the same weight such that the results could be compared. Note that this experiment was only carried through for three I_T-channel distribution ($g_{T_{Zom}}$ was omitted from the recordings, see discussion).

The results of the measurements for inputs i) - iii) are summarized in the figures 5.6, 5.8 and 5.7.

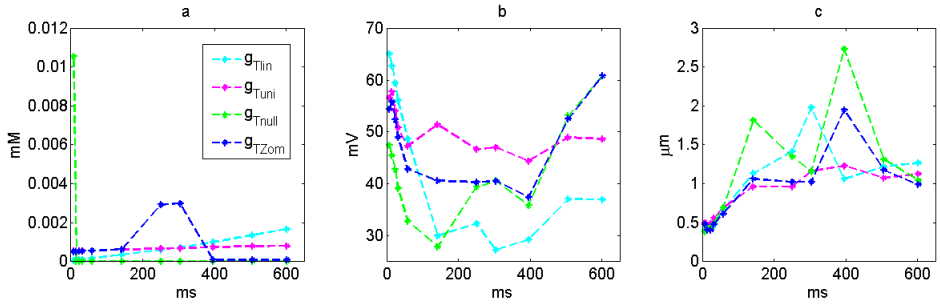

Figure 5.6: **Input i** : **a**) Amplitude of calcium elevation resulting from a selected spike in burst **b**) Amplitude of a selected spike in a burst **c**) Width of a selected spike in burst

5.3.1 AP propagation did not depend strongly on I_T-channel distribution

I found that action potentials successfully invaded the distal dendrites regardless of the I_T-channel distribution (see figure 5.7 b). Also, the shape of the action potential broadened slightly as distance from soma grew. This can be seen in figure 5.7 c). These features were not greatly effected by the I_T-channel distribution.

The calcium increase that was evoked by the action potential propagation tended to be highest at the points where the density of I_T-channels was highest (see figure 5.7 a)), and the voltage levels are independent of the I_T-channel distributions.

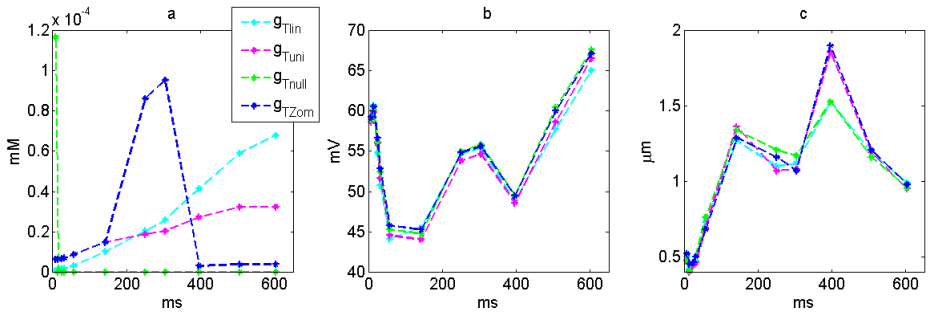

Figure 5.7: **Input iii** : **a**) Amplitude calcium elevation of a selected AP **b**) Amplitude of a selected AP **c**) Width of a selected AP

5.3.2 I_T-distribution greatly affects propagation of calcium spikes and EPSPs

When comparing how the propagation of a calcium spike depended on the distribution, interesting results were found. Also in this case, the calcium amplitude followed the I_T-distribution a great deal (see figure 5.8 a).
Counter to the findings in the previous section, I found the voltage level in distal dendrites to be strongly dependent on the distribution of I_T-channels. In figure 5.8 b) we can see that the voltage level follows the distribution, i.e., increases linearly for g_{lin}, and is uniform for g_{uni} and so on.

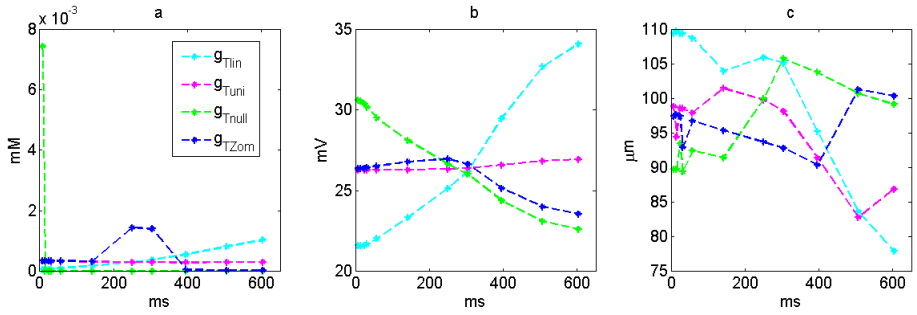

Figure 5.8: **Input ii** : **a**) Amplitude of calcium elevation resulting form a calcium spike **b**) Amplitude of a calcium spike **c**) Width of a calcium spike

Table 5.2 below shows an overview of the ratio between amplitudes of soma and averaged amplitudes of distal dendrites for a calcium spike:

Table 5.2: Ratio of voltage amplitudes for ca-spike

Distribution	$\frac{AMPsoma}{AMPdistdend}$ for ca-spike
g_{lin}	0.78
g_{uni}	1.00
g_{zero}	1.19

I can here see that the linearly increasing I_T-channel distribution is optimal for propagation of a somatic signal input. This is illustrated in figure 5.8 b), where we can see that the distribution g_{lin} leads to the highest amplitude in the distal dendrites.

5.3.3 Somatic and dendritic responses of synapses in distal dendrites

Synapses in the distal dendrites cause excitatory post synaptic potentials (EPSPs) that propagate towards the soma. For a synapse placed at the tip of a distal dendrite

(input iv, described in figure 5.9), I recorded the somatic and dendritic voltage amplitude.

The table below shows an overview of the ratios between between amplitudes of distal dendrites and amplitudes of soma for a synaptic input.

Table 5.3: Ratio of voltage amplitudes for synapse

Distribution	$\frac{AMPdistdent}{AMPsoma}$ for synapse
g_{lin}	11.6
g_{uni}	19.3
g_{zero}	19.6
g_{Zom}	19.5

The distribution g_{lin} is clearly optimal for the somatic response to a synaptic input, and thus is optimal for communication going in both directions between the soma and the distal dendrites.

The results of the measurements for input iv) are summarized in figure 5.9. The top figure shows measurements of voltage amplitude of the response signal to subthreshold synaptic input, while the bottom figure shows the measurements of calcium elevations.

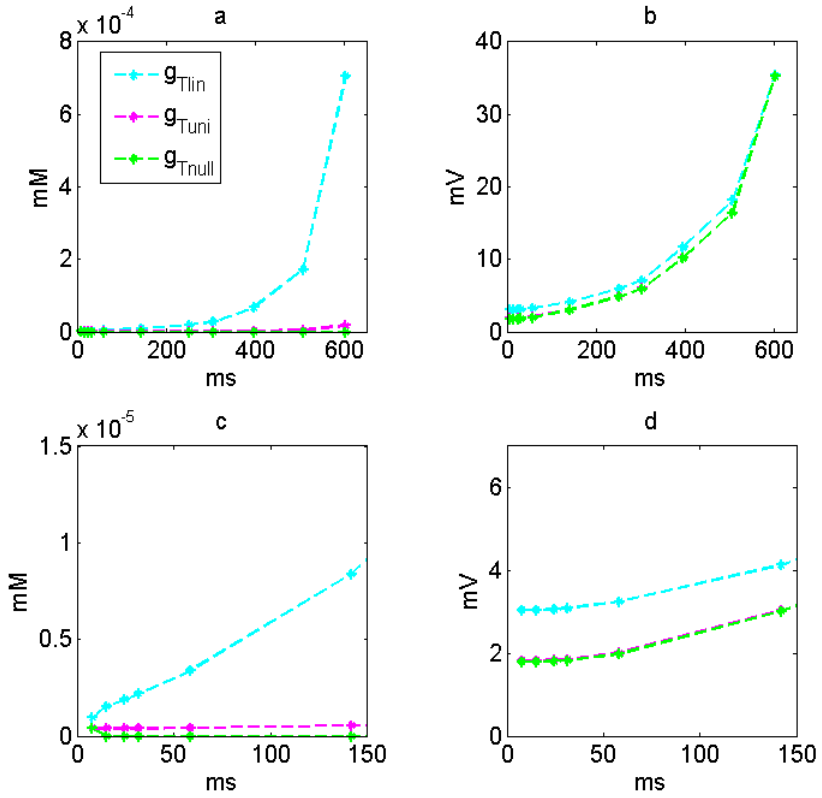

Figure 5.9: **Input iv** : **a**) Amplitude of a voltage elevation resulting from synapse in distal dendrite **b**) Close up of a) near soma **c**) Amplitude of calcium elevation. Note that signals are initiated on the right hand side of the figure, and propagate towards the left. **d**) Close up of b) near soma

Chapter 6

Discussion

A series of simulations have been run in this thesis, with an attempt to predict the consequences varying I_T-channel distributions have on somatic and dendritic calcium and voltage levels. I now pose the question: which of these predictions are in most agreement with experimental recordings?

6.1 Main conclusions

The linearly increasing I_T-channel distribution was found to optimal for a outward propagating calcium spike initiated in the soma. This supports the experimental findings of Parajuli et al. [15].

It has been suggested that the existence of synapses in distal dendrites enables interneurons to modulate the activity of thalamocortical cells, helping balance the information relay to the cortex [19]. This linearly increasing distribution of I_T-channels was also found to be optimal for the propagation of a synaptic impulse towards the soma. The increased channel density in distal dendrites may be a means of amplifying somatic input, thus helping to increase the activation of synapses at distal locations.

6.2 Reducing the morophology

I initially considered doing simulations on a simplified morphology, basing the model structure on the 3-compartment model of Zomorrodi et al. [18], and combining it with parameters and properties from Halnes et al. [9]. However, most methods for simplifying the morphology require the assumption of dendritic symmetry- that all dendrites have approximately have the same length and branch in the same way. As they also imply a simulational symmetry, these reduced models are good for either studying how somatic signals are spread outwards in the dendrites, or how the soma responses to simultaneous activation of a large number of synapses that are assumed to be homogeneously distributed across the dendrites.
The synapses to the INs that are studied in this paper are retinal synapses, and tend to be quite strong, so activation of 1 - 4 synapses is sufficient for driving the soma

to fire action potentials. As the goal was to study the the response of single synaptic inputs, the problem to investigate is asymmetric. Thus, the methods for simplifying the morphology were not applicable in this case.

6.3 Limitations of the study

Every model of a biological mechanism will be a simplification on some scale, where assumptions and compromises on what aspects to include are made. Only 3 ion channels are included in this model, as opposed to he original model's 7, omitting ion channels that play a key role for specific firing properties [9]. These simplifications were made so that the role of the I_T-channel could be studied in isolation, and I believe that the results reveal relations that are qualitatively important. However, I am aware that the effects that would occur if other channels were included are missing. The firing patterns would differ if other channels were used, and the possibility of these changing the results, can not be excluded.

Some simulation results are only shown for the distributions g_{lin}, g_{uni} and g_{zero}. This is due to an error in the coding for the g_{Zom} distribution that was discovered too late in the process to embark on the simulations.

The scope of the study was also relatively small, as experiments were only carried out on a single neuron morphology, and only investigating a few dendritic pathways. Conclusions are hard to make with such a limited vantage point

6.4 Comparing results to experimental findings

Different conclusions regarding the I_T-channel distribution have been reached in experimental studies. Munsch et al. [21] studied the intracellular calcium concentration dynamics of interneurons in rat LGNs, and their findings reflected a uniform distribution of I_T-channels. On the other hand, Parajuli et al. [15] came to a different conclusion in their studies on distribution of a subunit of I_T-channels, finding the channel density to be higher in proximal dendrites, and decrease towards the distal dendrites.

Some of the results in my simulations were in disagreement with experimental findings:

· Although previous experimental results have indicated that synaptic induced action potentials always originate in proximity to the soma [2], I found that sufficiently strong synaptic stimuli could lead to a burst originating in the synaptic region (see figure 5.2).

· The linearly increasing I_T-channel distribution predicted that an action potential or calcium spike propagating outward from the soma would lead to an elevation in calcium concentration in the dendrites (see figure 5.7 and 5.8). This is in contradiction with experimental results that have indicated dendritic calcium levels to remain unvaried with distance from soma. [5]

The results of the uniform I_T-channel distribution on the other hand gave rise to results that were qualitatively similar to the findings of Acuna-Goycolea et al. This may indicate that a uniform distribution of I_T-channels is in best agreement with experiments on dendritic signal propagation.

6.5 Future work

As the distribution g_{Zom} has been omitted from some of the simulations, these need to be tested.

A natural continuation of this thesis, before expanding the project, would be to repeat the simulations on different morphologies, and also several more dendritic pathways on the same morphology. This would contribute to strengthening the conclusions of the study.
It would also be interesting to repeat the simulations with slight variations in strengths of the input signals, as to assure that the results are not specific to the signal strengths used.

The passive properties (e.g. membrane resistance) and ion channel densities will likely vary from cell to cell, they will even vary within the same cell type. The results should be qualitatively reproduced for other parameterizations of the model. A parameter sensitivity analysis would also be an interesting focus for future work.

Further, studies should also be carried out including more ion channels. Here, the most natural candidate to choose would be the L-type calcium channel I_L, as this would directly impact the dendritic calcium levels.

Bibliography

[1]

[2]

[3] Daniel Ulrich John Huguenard Alain Destexhe, Mike Neubig. Dendritic low-threshold calcium currents in thalamic relay cells. *The Journal of Neuroscience*.

[4] Robert J. Demarest David A. Ruggerio Charles R. Noback, Norman L. Strominger. *The Human Nervous System - Structure and Function*. Humana Press, Totowa, New Jersey, 2005.

[5] Wade G. Regehr Claudio Acuna-Goycolea, Stephan D. Brenowitz. Active dendritic conductances dynamically regulate gaba release from thalamic interneurons. *Neuron*.

[6] David Cofer. Neuron diagram. `http://www.mindcreators.com/NeuronBasics.htm`. Accessed May 7, 2012.

[7] Life Science Databases. File:thalamus.png. `http://en.wikipedia.org/wiki/File:Thalamus.png`. Accessed November 17, 2011.

[8] Peter Dayan and L. F. Abbott. *Theoretical Neuroscience*. The MIT Press, Cambridge, Massachussets, 2001.

[9] Paul Heggelund Gaute T. Einevoll Michele Migliore Geir Halnes, Sigita Augustinaite. A multi-compartment model for interneurons in the dorsal lateral geniculate nucleus. *PLoS Computational Biology*, 7(9).

[10] Thomas Budde Hans-Christian Pape, Thomas Munsch. Novel vistas of calcium-mediated signalling in the thalamus. *Pflugers Archiv - European Journal of Physiology*.

[11] Eugene M. Izhikevich. *Dynamical Systems in Neuroscience - The Geometry of Excitability and Bursting*. The MIT Press, Cambridge, Massachussets, 2007.

[12] W. W. Lytton J. J. Zhu, D. J Uhlrich. Burst firing in identified rat geniculate interneurons. *Neuroscience*.

[13] W. W. Lytton J. J. Zhu, D. J Uhlrich. Properties of hyperpolarization-activated cation current in interneurons in the rat lateral geniculate nucleus. *Neuroscience*.

[14] Christof Koch and Idan Segev. *Methods in Neuronal Modeling - From Ions to Networks*. The MIT Press, Cambridge, Massachussets, second edition, 1998.

[15] Masahiko Watanabe Ryuichi Shigemoto Laxmi Kumar Parajuli, Yugo Fukazawa. Subcellular distribution of alpha 1g subunit of $t - type$ calcium cahennel in the mouse dorsal lateral geniculate nucleus. *The Journal of Comparatice Neurology*.

[16] Inc MicriBrightField. Neurolucida. `http://www.mbfbioscience.com/neurolucida`. Accessed May 7, 2012.

[17] M.L. Hines N.T. Carnevale. What is neuron? `http://www.neuron.yale.edu/neuron/what_is_neuron`. Accessed April 4, 2010.

[18] Igor Timofeev Reza Zomorrodi, Helmut Kroger. Modelling thalamacortical cell: impact of ca2+ channel distribution and cell geomtry on firing pattern. *Frontiers in Computational Neuroscience*.

[19] S. Murray Sherman. Interneurons and triadic cirfuitry of the thalamus. *Trends in Neurosciences*.

[20] S. Murray Sherman and R. W. Guillery. *Exploring the Thalamus and Its role in Cortical Function*. The MIT Press, Cambridge, Massachussets, second edition, 2006.

[21] Hans-Christian Pape Thomas Munsch, Thomas Budde. Voltage-activated intracellular calcium transients in thalamic relay cells and interneurons. *NeuroRepor*.

Appendix A

HOC code for NEURON Simulations

A.1 it2.mod

```
TITLE Low threshold calcium current
:
:   Ca++ current responsible for low threshold spikes (LTS)
:
:   Written by Alain Destexhe, Salk Institute, Sept 18, 1992
:   Modified by Geir Halnes, Norwegian University of Life Sciences, June 2011:
:
:     - Kinetics adapted to LGN interneuron data from Broicher et al.: Mol Cell
:        Neurosci 36: 132-145, 2007. using Q10 values of 3 and 1.5 for activation/
:        inactivation.
:     - Activation variable shifted 8mV to account for dLGN interneuron data in
:        Halnes et al. 2011


INDEPENDENT {t FROM 0 TO 1 WITH 1 (ms)}

NEURON {
SUFFIX it2
USEION Ca READ Cai, Cao WRITE iCa VALENCE 2
RANGE gcabar, g
GLOBAL m_inf, tau_m, h_inf, tau_h, shift2, sm, sh, phi_m, phi_h, hx, mx, shift1
}

UNITS {
(molar) = (1/liter)
(mV) = (millivolt)
(mA) = (milliamp)
(mM) = (millimolar)
FARADAY = (faraday) (coulomb)
R = (k-mole) (joule/degC)
}
```

```
PARAMETER {
v (mV)
celsius = 36 (degC)
gcabar = 8.5e-6 (mho/cm2)
        hx      = 1.5
        mx      = 3.0
Cai = 5e-5 (mM) : Initial Ca concentration
Cao = 2 (mM) : External Ca concentration

: GH, parameters fitted to Broicher et al. 07 - data
minf1 = 46.2
hinf1 = 69.7
taum1 = 5.4
taum2 = 125.7
taum3 = -19.7
taum4 = -0.54
taum5 = 13
tauh1 = 21
tauh2 = 22.2
tauh3 = 9.1
tauh4 = 362.9
tauh5 = 46.9
        sm = 8.7
        sh = 6.4
shift1 = -8  (mV) : Halnes et al. 2011
        shift2  = 0     (mV) : Halnes et al. 2011
}


STATE {
m h
}

ASSIGNED {
iCa (mA/cm2)
g       (mho/cm2)
carev (mV)
m_inf
tau_m (ms)
h_inf
tau_h (ms)
phi_m
phi_h
}
```

```
BREAKPOINT {
SOLVE castate METHOD cnexp
g = gcabar * m*m*h
iCa = g * ghk(v, Cai, Cao)
}

DERIVATIVE castate {
evaluate_fct(v)
m' = (m_inf - m) / tau_m
h' = (h_inf - h) / tau_h
}

UNITSOFF
INITIAL {
VERBATIM
Cai = _ion_Cai;
Cao = _ion_Cao;
ENDVERBATIM
:
phi_m = mx ^ ((celsius-23.5)/10)
phi_h = hx ^ ((celsius-23.5)/10)

evaluate_fct(v)
m = m_inf
h = h_inf
}

PROCEDURE evaluate_fct(v(mV)) {
m_inf = 1.0 / ( 1 + exp(-(v+shift1+minf1)/sm) )
h_inf = 1.0 / ( 1 + exp((v+shift2+hinf1)/sh) )
tau_m = (taum1+1.0/(exp((v+shift1+taum2)/(taum3))+exp((v+shift1+taum4)/
taum5)))/ phi_m
tau_h = (tauh1+1/(exp((v+shift2+tauh2)/tauh3)+exp(-(v+shift2+tauh4)/tauh5)))/
phi_h
}

FUNCTION ghk(v(mV), Ci(mM), Co(mM)) (.001 coul/cm3) {
LOCAL z, eci, eco
z = (1e-3)*2*FARADAY*v/(R*(celsius+273.15))
eco = Co*efun(z)
eci = Ci*efun(-z)
:high Cao charge moves inward
:negative potential charge moves inward
ghk = (.001)*2*FARADAY*(eci - eco)
}
```

```
FUNCTION efun(z) {
if (fabs(z) < 1e-4) {
efun = 1 - z/2
}else{
efun = z/(exp(z) - 1)
}
}
UNITSON
```

A.2 loi04.hoc

```
: GH, August 2010
: Modified by JC, February 2012
: - Shift in it2.mod set to 0

// GH, August 2010
load_file("nrngui.hoc")
cvode_active(1)
load_file("091008A2.hoc") // uses Heggelund morphoplogy
xopen("fixnseg.hoc")

//objref stim, syn, s, nc       //vanlig (ikke-synapse) kode

nsyn=6
//nsyn=4                                          //synapsekode
objref stim, syn[nsyn], s[nsyn], nc[nsyn]      //synapsekode

dt = 0.1
celsius = 36.0

// From fitting of passive properties:
rall = 113 //most people find something like this
cap = 1.1
Rm = 45000
Vrest = -69
Epas = -71.6

// Channel densities & shifts (for additional channels see May_dends.hoc)
gna =  0.09
nash = - 50.3
gkdr = 0.5
kdrsh = -48
gahp =  0//0.00013
gcat=8.5e-6
```

```
gcal=0.0013
ghbar=0 //5e-6
catau = 50
gcanbar = 0// 1e-7

// Channel distribution (ratio: g_dend/g_soma)
hhdendfac = 0.1
ihdendfac = 1
ldendfac = 0.25
iahpdendfac = hhdendfac
itinc = 2.39/60
icaninc = itinc

// Insert channels:
forall {insert pas e_pas=Vrest g_pas=1/Rm Ra=rall cm=cap}
forall {
insert iar ghbar_iar=ghbar*ihdendfac // Ih-cation channel, slow, Zhu
insert Cad // Single calsium pool, Zhu et al.99
insert ical // L-type Ca-current, using pool in Cad
insert it2 // t-type Ca- current, using pool in Cad
insert iahp // potassium current, slow, Ca-dependent, Zhu et al.99
insert hh2 ena=50 ek=-90 //
insert ican // Zhu et al. 99a
}


// Initialize
proc init() {
access soma
forall {v=Vrest e_pas=Epas}
        forall {insert pas e_pas=Epas g_pas=1/Rm Ra=rall cm=cap}

forall {
gnabar_hh2 = gna*hhdendfac  vtraubNa_hh2 = nash
        gkdrbar_hh2 = gkdr*hhdendfac vtraubK_hh2 = kdrsh
pcabar_ical = gcal*ldendfac
gkbar_iahp = gahp*iahpdendfac
ghbar_iar = ghbar*ihdendfac
gcabar_it2 = gcat*(1 + itinc*distance(1)) // 0// gcat*1 //
gbar_ican = gcanbar*(1 + itinc*distance(1)) // 0// gcanbar*1 //
}

soma {
gnabar_hh2 = gna vtraubNa_hh2 = nash
gkbar_hh2 = gkdr vtraubK_hh2 = kdrsh
gcabar_it2 = gcat
```

```
pcabar_ical = gcal
gkbar_iahp = gahp
ghbar_iar = ghbar
gbar_ican = gcanbar
}

GCATOT = 0
soma {
    gcabar_it2 = gcat
    GCATOT = GCATOT + area(0.5)*gcabar_it2
}

for i = 0, 104  {
access dend[i]
segmentL = 1/nseg // lengde, relativt til totallengden av seksjon

for segmentNR = 1, nseg {
midten = segmentNR/nseg - segmentL/2 //
gcabar_it2(midten) =gcat*(1 + itinc*distance(midten)) //  0 // gcat*1
arealet = area(midten) // areal av segmentet
GCATOT = GCATOT + gcabar_it2(midten)*arealet
}

}

/*
NY For Zomorrodi
GCATOT = 0
soma {
    gcabar_it2 = gcat*1.7
    GCATOT = GCATOT + area(0.5)*gcabar_it2
}

for i = 0,9{
access dend[i]
segmentL = 1/nseg
for segmentNR = 1, nseg {
midten = segmentNR/nseg - segmentL/2
gcabar_it2(midten) = gcat*1.7
arealet = area(midten) // areal av segmentet
GCATOT = GCATOT + gcabar_it2(midten)*arealet
}
}

for i = 11,11{
access dend[i]
```

```
segmentL = 1/nseg
for segmentNR = 1, 7 {
midten = segmentNR/nseg - segmentL/2
gcabar_it2(midten) = gcat*1.7
arealet = area(midten) // areal av segmentet
GCATOT = GCATOT + gcabar_it2(midten)*arealet
}
for segmentNR = 8, nseg {
midten = segmentNR/nseg - segmentL/2
gcabar_it2(midten) = gcat*7.81
arealet = area(midten) // areal av segmentet
GCATOT = GCATOT + gcabar_it2(midten)*arealet
}
}

for i = 12,14{
access dend[i]
segmentL = 1/nseg
for segmentNR = 1, nseg {
midten = segmentNR/nseg - segmentL/2
gcabar_it2(midten) = gcat*7.81
arealet = area(midten) // areal av segmentet
GCATOT = GCATOT + gcabar_it2(midten)*arealet
}
}

for i = 15,15{
access dend[i]
segmentL = 1/nseg
for segmentNR = 1, 2 {
midten = segmentNR/nseg - segmentL/2
gcabar_it2(midten) = gcat*7.81
arealet = area(midten) // areal av segmentet
GCATOT = GCATOT + gcabar_it2(midten)*arealet
}
for segmentNR = 3, nseg {
midten = segmentNR/nseg - segmentL/2
gcabar_it2(midten) = gcat*0.17
arealet = area(midten) // areal av segmentet
GCATOT = GCATOT + gcabar_it2(midten)*arealet
}
}

for i = 16,104{
access dend[i]
segmentL = 1/nseg
```

```
for segmentNR = 1, nseg {
midten = segmentNR/nseg - segmentL/2
gcabar_it2(midten) = gcat*0.17
arealet = area(midten) // areal av segmentet
GCATOT = GCATOT + gcabar_it2(midten)*arealet
//print arealet
}
}
*/

finitialize(Vrest)
      fcurrent()
// finitialize(Vrest)
      forall {taur2_Cad = catau} // Calcium decay
cvode.re_init()
}

access soma
freq=50
geom_nseg()
tot=0
forall {tot=tot+nseg}
distance()
print "total # of segments (50Hz): ",tot

stim = new IClamp(.5)
stim.del =100
stim.dur =1000
stim.amp =0.025

/*
// SYNAPSES (AMPA)
synweight1 = 0.001 // In muS
synweight2 = 0.001 // Dette definerer styrken paa synapsen.

for z=0, nsyn-1 {
// En for-loop som lager de fire synapsene
s[z] = new NetStim(.5)
s[z].start=2500
// Jeg valgte aa starte etter 2500s, etter opprinnelig stimulus
// for aa sammenligne. Kjoer simulering til e.g. 4000 sek.
s[z].number=1
s[z].noise=0
syn[z] = new Exp2Syn(.5)
// Synapsestroem = sum av to eksponensialfunksjoner. Innebygd Neuronfunksjon.
syn[z].tau1=0.5 // Tidskonstant for foerste eksponensialfunksjon
```

```
syn[z].tau2=2 // Tidskonstant for den andre.
syn[z].e=10 // Reverseringspot. for AMPASYNAPSE.
}

// UNDER PLASSERES DE FIRE SYNAPSENE PAA FIRE ULIKE STEDER
dend[99] {syn[0].loc(0.5)}
nc[0] = new NetCon(s[0], syn[0], 0,0, synweight1)
dend[17] {syn[1].loc(0.5)}
nc[1] = new NetCon(s[1], syn[1], 0,0, synweight2)
dend[55] {syn[2].loc(0.5)}
nc[2] = new NetCon(s[2], syn[2], 0,0, synweight2)
dend[37] {syn[3].loc(0.5)}
nc[3] = new NetCon(s[3], syn[3], 0,0, synweight2)
*/


//ALTERNATIV SYNAPSEKODE
synweight1 = 0.001 // In muS
synweight2 = 0.001 // Dette definerer styrken paa synapsen.

for z=0, nsyn-1 {
// En for-loop som lager de SEKS synapsene
s[z] = new NetStim(.5)
s[z].start=2500
// Jeg valgte aa starte etter 2500s, etter opprinnelig stimulus
// for aa sammenligne. Kjoer simulering til e.g. 4000 sek.
s[z].number=1
s[z].noise=0
syn[z] = new Exp2Syn(.5)
// Synapsestroem = sum av to eksponensialfunksjoner. Innebygd Neuronfunksjon.
syn[z].tau1=0.5 // Tidskonstant for foerste eksponensialfunksjon
syn[z].tau2=2 // Tidskonstant for den andre.
syn[z].e=10 // Reverseringspot. for AMPASYNAPSE.
}

// UNDER PLASSERES DE FIRE SYNAPSENE PAA FIRE ULIKE STEDER
dend[8] {syn[0].loc(0.5)}
nc[0] = new NetCon(s[0], syn[0], 0,0, synweight1)
dend[3] {syn[1].loc(0.5)}
nc[1] = new NetCon(s[0], syn[1], 0,0, synweight1)
dend[55] {syn[2].loc(0.5)}
nc[2] = new NetCon(s[2], syn[2], 0,0, synweight2)
dend[37] {syn[3].loc(0.5)}
nc[3] = new NetCon(s[3], syn[3], 0,0, synweight2)
dend[17] {syn[4].loc(0.5)}
nc[4] = new NetCon(s[1], syn[4], 0,0, synweight2)
```

```
dend[99] {syn[5].loc(0.5)}
nc[5] = new NetCon(s[0], syn[5], 0,0, synweight1)
```